Deformation of the western Andes at 20–22°S: a contribution to the quantification of crustal shortening

Tania Habel, Robin Lacassin, Martine Simoes, Daniel Carrizo, Germán Aguilar

Manuscript submitted to Tectonics :

Deformation of the western Andes at ~20–22°S: a contribution to the quantification of crustal shortening

Tania Habel – Université de Paris, Institut de physique du globe de Paris, CNRS, F-75005 Paris, France – **habel@ipgp.fr**

Robin Lacassin – Université de Paris, Institut de physique du globe de Paris, CNRS, F-75005 Paris, France – **lacassin@ipgp.fr**

Martine Simoes – Université de Paris, Institut de physique du globe de Paris, CNRS, F-75005 Paris, France – **simoes@ipgp.fr**

Daniel Carrizo – GeoEkun SpA, Santiago 7500593, Chile – **carrizo@geoekun.com**

Germán Aguilar – Advanced Mining Technology Center, Facultad de Ciencias Físicas y Matemáticas, Universidad de Chile, Avenida Tupper 2007, Santiago, Chile – **german.aguilar@amtc.cl**

This a non peer-reviewed paper.
This manuscript has been submitted for publication to Tectonics on 2020-12-17

Any comments can be sent to the corresponding authors: **habel@ipgp.fr**

Deformation of the western Andes at ~20–22°S: a contribution to the quantification of crustal shortening

T. Habel[1], R. Lacassin[1], Martine Simoes[1], D. Carrizo[2,3], and G. Aguilar[2]

[1]Université de Paris, Institut de physique du globe de Paris, CNRS, F-75005 Paris, France

[2]Advanced Mining Technology Center, Facultad de Ciencias Físicas y Matemáticas, Universidad de Chile, Avenida Tupper 2007, Santiago, Chile

[3]now at GeoEkun SpA, Santiago 7500593, Chile

Corresponding author: Tania Habel (habel@ipgp.fr)

Key Points:

- Kinematics of shortening of the West Andean Fold-and-Thrust-Belt and the Andean Basement Thrust at ~20–22°S
- Multi-kilometric shortening across the western Andes after ~68 Ma, implying significant contribution in the early stages of Andean orogeny
- Significant slowing-down of deformation rates after ~29 Ma (and starting possibly earlier)

Abstract

The Andes are an emblematic active Cordilleran orogen. It is admitted that mountain-building in the Central Andes, at ~20°S, started ~50–60 Myr ago, along the subduction margin, and propagated eastward. In general, the structures sustaining the uplift of the western flank of the Andes are dismissed, and their contribution to mountain-building remains poorly solved. Here, we focus on two sites along the western Andes at 20–22°S, in the Atacama Desert, where structures are well exposed. We combine mapping from high-resolution satellite images with field observations and numerical trishear forward modeling to provide quantitative constraints on the kinematic evolution of the western Andes. Our results confirm the existence of two main structures: (1) the Andean Basement Thrust, a west-vergent thrust placing Andean Paleozoic basement over Mesozoic strata; and (2) the west-vergent West Andean Fold-and-Thrust-Belt, deforming primarily Mesozoic units. Once restored, we estimate that both structures accommodate together at least ~6–9 km of shortening across the sole ~7–17 km-wide outcropping fold-and-thrust-belt. This multi-kilometric shortening represents only a fraction of the total shortening accommodated along the whole western Andes. The timing of the recorded main deformation can be bracketed sometime between ~68 and ~29 Ma – and possibly between ~68 and ~44 Ma – from dated deformed geological layers, with a subsequent significant slowing-down of shortening rates. Our results therefore reveal that the contribution of the structures of the West Andes can no longer be neglected, in particular at the earliest stages of Andean mountain-building.

1 Introduction

One of the most active convergent plate boundaries is located along the western margin of South America (Figure 1). There, the oceanic Nazca plate plunges beneath the South American continent, with a convergence rate currently of ~8 cm/yr at ~20ºS, according to the NUVEL-1A model (DeMets et al., 1994). The major part of this convergence is absorbed by the subduction megathrust in the form of large earthquakes (magnitude Mw≥8). A small fraction of this convergence – presently about 1 cm/yr at 20°S (e.g., Brooks et al., 2011; Norabuena et al., 1998) – contributes to the deformation of the upper plate over millions of years and to the formation of one of the largest reliefs at the Earth's surface: the Andean Cordilleras and the Altiplano-Puna plateau in between (Figure 1).

Andean mountain-building processes are still a matter of debate. A widely accepted model explains the building of the current topography and the crustal thickness of the whole orogen as the result of thrusting propagating eastward over time and concentrated presently on the eastern Andean front, whereas the western flank is described as a passive monoclinal-like crustal-scale flexure (e.g., Isacks, 1988; Lamb, 2011, 2016). However, in the late 1980's, Mpodozis and Ramos (1989) suggested that the Andes-Altiplano was a bivergent orogen with east-vergent structures on the eastern side (along the Sierras Subandinas) and west-vergent thrusting on the western margin (along the Cordillera Domeyko). Later, other authors described west-vergent thrusts at several localities along the western Andean flank (e.g., Charrier et al., 2007; Farías et al., 2005; Garcia & Hérail, 2005; Muñoz & Charrier, 1996; Victor et al., 2004), but they generally gave to these thrusts a minor role in the building of the whole orogen by considering them as secondary backthrusts. A recent and still debated model actually assigns a more important role to these structures, with a west-verging fold-and-thrust-belt (fold-and-thrust-belt hereafter simplified as FTB) along the west Andean flank, thus depicting again the Andes-Altiplano as a bivergent orogen (Armijo et al., 2010, 2015; Riesner et al., 2018). The contribution of this western west-verging FTB to crustal Andean shortening and thickening has been evaluated and quantified at the latitude of Santiago de Chile, ~33°30'S (Armijo et al., 2010; Riesner et al., 2017, 2018, 2019). There, the orogen is relatively younger and structurally more simple, with a narrower width (Figure 1) and less structural units than in the Central Andes further north. It has been proposed that the FTB emerging along the west Andean front roots on a deeper thrust ramp – the West Andean Thrust (or WAT) – that would represent the primary

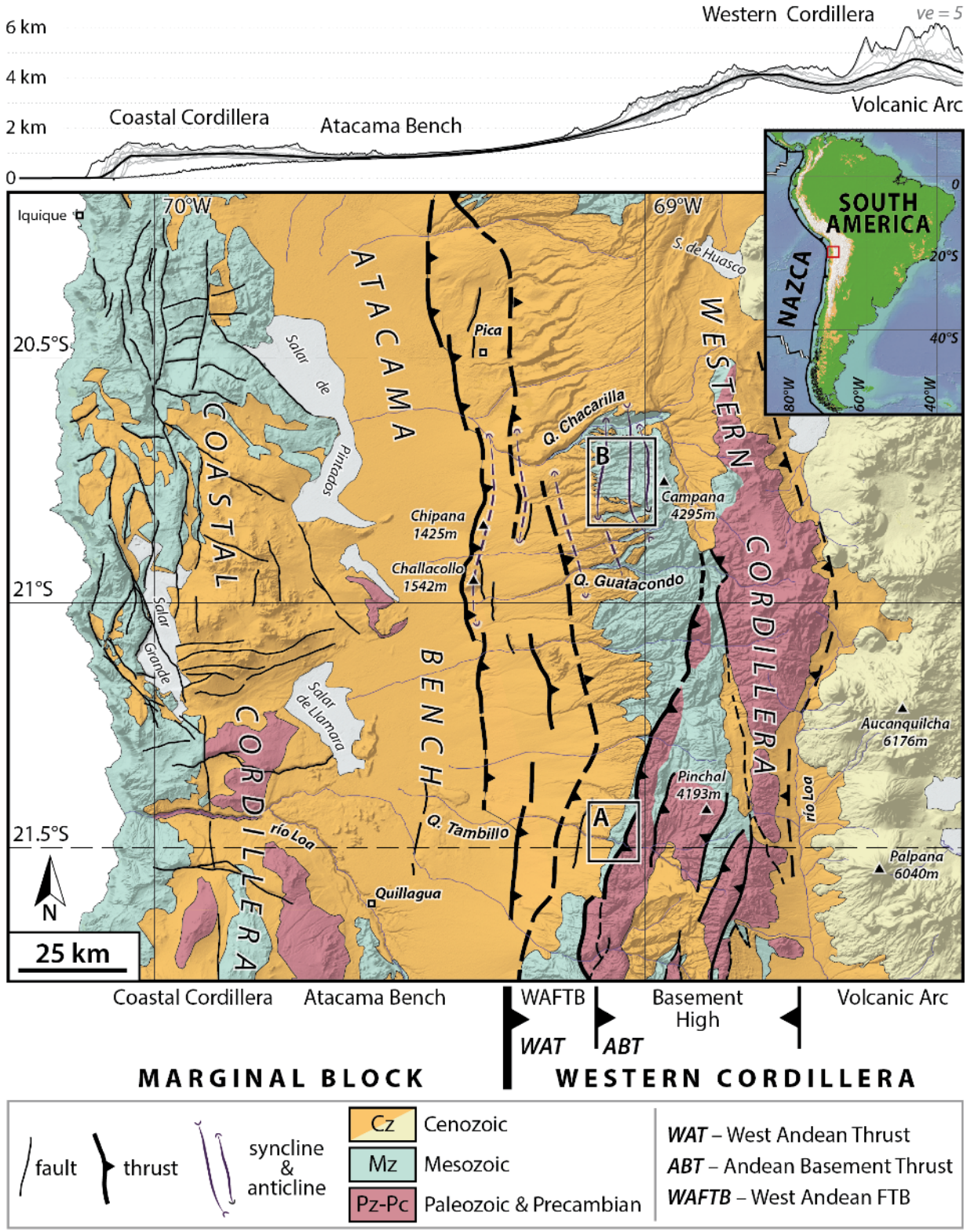

Figure 1. Simplified geological and structural map of the western Central Andes at ~20–22ºS, Northern Chile (modified from Armijo et al., 2015), and average topographic profile (top; ve: vertical exaggeration). The two main structural ensembles are here the Marginal Block and the Western Cordillera. The Marginal Block encompasses the Coastal Cordillera and the longitudinal valley of the Atacama Bench (or Central Depression). The Western Cordillera includes the West Andean Fold-and-Thrust-Belt (WAFTB) and Basement High (Cordillera Domeyko), and the modern volcanic arc. A large part of the WAFTB is hidden beneath blanketing Cenozoic deposits and only outcrops in few places. The Andean Basement Thrust (ABT) separates the WAFTB and the Basement High of the Western Cordillera. The location of Figures 4 and 9 is given by black boxes (A and B, respectively). Inset: Location of the map (red box) within the Central Andes along the South American Continent. WAT: West Andean Thrust (after Armijo et al., 2015); FTB: Fold-and-Thrust-Belt; Cz: Cenozoic; Mz: Mesozoic; Pz-Pc: Paleozoic and Precambrian.

crustal-scale structure on which the orogeny initiated at ~33°30'S (Armijo et al., 2010; Riesner et al., 2018, 2019).

In contrast, the contribution of similar west-vergent structures further north, at ~20–22°S (in the so-called Bolivian Orocline), is probably small compared to the total shortening across the entire Andes-Altiplano system, but their role at the start of orogenic building, ~50 Myr ago, may have been similarly important (Armijo et al., 2015). At this latitude, Victor et al. (2004) have shown the existence of west-vergent thrusts rooting on a deep decollement dipping eastward beneath the western Andes. They also estimated that these structures absorbed a shortening of ~3 km. However, this relatively minor shortening only characterizes the deformation affecting the post ~29 Ma Altos de Pica Formation deposited above the Choja erosional surface (or Choja Pediplain). The deformation of the Mesozoic series beneath this surface appears much stronger (Armijo et al., 2015; Blanco & Tomlinson, 2013) but remains to be precisely described and quantified. One of the difficulties in such quantification is that a very large part of the deformation is hidden under blanketing mid-upper Cenozoic deposits and volcanics (Armijo et al., 2015; Farías et al., 2005; SERNAGEOMIN, 2003; Victor et al., 2004). A quantitative analysis of this deformation and its kinematics is only possible at the few sites along the western flank where deformed Mesozoic series crop out and which are accessible despite the hostile desert conditions in North Chile.

In this study, we provide quantitative data to better constrain the geometry of structures, the shortening they accommodated and their kinematics of deformation over time in two of the few areas along the west Andean front where erosion of the Cenozoic units allows for exposures of the underlying deformed Mesozoic layers (Figure 1). The Pinchal area, at ~21°30'S, exhibits a major west-vergent thrust that brings the Paleozoic basement of the Cordillera Domeyko over a FTB of Mesozoic units. These structures have never been described in detail. In the Quebrada Blanca zone, ~80 km further north, the excellent exposure of the FTB affecting the Mesozoic series allows for a more quantitative estimate of the shortening and of the timing of the main deformation episodes. Despite our detailed and quantitative approach, these two study areas only give a limited minimal vision of total deformation of this region, as their spatial extent remains minor at the scale of the whole western Andean flank (Figure 1). We find that the shortening of these structures is multi-kilometric, revealing that the contribution of the west Andean flank to Andean mountain building is not negligible. Additionally, we show that the main recorded

deformation occurred sometime between ~68 and ~29 Ma (and possibly between ~68 Ma and ~44 Ma), further emphasizing that these structures mostly participated to the early stages of mountain-building.

2 Geological Context of the Andes (~20–22°S)

2.1 General geological framework

The Central Andean mountain-belt extends parallel to the Peru–Chile trench (Figure 1), where the Nazca oceanic plate subducts slightly obliquely beneath the South American continent. Spreading out north–south over several thousands of kilometers, the morpho-tectonic structure of the belt varies not only across the range, but also along its ~north–south axis.

At ~20–22°S, the mountain-belt is characterized by its largest width (>650 km), highest average elevation (~4–4.5 km above sea level, hereafter a.s.l., Figure 1), thickest crust (70–80 km, e.g., Tassara et al., 2006; Wölbern et al., 2009; Yuan et al., 2000) and greatest total shortening (>300 km, e.g., Anderson et al., 2017; Elger et al., 2005; McQuarrie et al., 2005; Sheffels, 1990). Here, the Andean margin along the western border of the continent is described by three major morpho-tectonic ensembles, which are, from west to east (Figure 1): (1) the subduction margin (including the Peru–Chile Trench, the oceanward forearc, and the Coastal Cordillera that reaches altitudes >1 km and that corresponds to the former Mesozoic volcanic arc); (2) the Atacama Bench or Central Depression (at an altitude of ~1 km, corresponding to a modern continental forearc basin, particularly well expressed in the morphology and topography in North Chile) and (3) the strictly speaking Andean orogen, including the current volcanic arc and the Altiplano plateau reaching elevations over 4000 m a.s.l. at ~20°S (e.g., Charrier et al., 2007; McQuarrie et al., 2005; Oncken et al., 2006). Following the terminology of Armijo et al. (2010, 2015), the morpho-tectonic units located west of the Andean orogen constitute the Marginal Block (i.e. the oceanward forearc, the Coastal Cordillera and the Atacama Bench).

At ~20–22°S latitude, the Andean orogen itself is composed of several major tectono-stratigraphic ensembles, which are, from west to east: (1) the Western Cordillera (Figure 1), including the Cordillera Domeyko and the modern volcanic arc; (2) the Altiplano Plateau, a high-elevation internally drained low-relief basin; (3) the Eastern Cordillera, a bi-vergent portion of the East Andean FTB; (4) the Interandean zone (or Cordillera Oriental); and (5) the

Subandean ranges, east of which the South American craton underthrusts the Andes (e.g., Armijo et al., 2015; Isacks, 1988; McQuarrie et al., 2005; Oncken et al., 2012). The Andean orogen is here tectonically and structurally delimited by two main bivergent thrust systems: the west-vergent West Andean Thrust (WAT) along the western flank, and the east-vergent East Andean Thrust (EAT) along the eastern flank (according to the terminology proposed by Armijo et al., 2015).

Although there exist indications of local minor deformation during the Cretaceous, the building of the Andean mountain-belt stricto sensu proceeded during the past ~50 Myr at ~20–22ºS and was associated with crustal shortening and thickening (e.g., Armijo et al., 2015; Barnes et al., 2008; Charrier et al., 2007; DeCelles et al., 2015; Faccenna et al., 2017; McQuarrie et al., 2005; Oncken et al., 2006). Based on the regional syntheses and reviews by McQuarrie et al. (2005), Oncken et al. (2006), Charrier et al. (2007) and Armijo et al. (2015), the across-strike growth of the orogen may be summarized as follows: (1) at ~70–50 Ma, the Mesozoic arc and backarc basin (formed during the early Andean cycle) is located at the position of the present-day forearc, and most of the current Andes shows mainly flat topography; (2) by ~50 Ma, orogenic growth initiates and deformation primarily affects the Western Cordillera and the western margin of the present-day Altiplano; (3) by ~30 Ma, main shortening vanishes in the Western Cordillera, and is transferred to the Eastern Cordillera, and subsequently to the Interandean Belt; (4) by ~20 Ma, deformation in the Eastern Cordillera and Interandean Belt ends as suggested by the development of erosional surfaces; (5) from ~10 Ma until present, deformation within the Subandean Belt proceeds while the Brazilian Craton underthrusts the Andes. It is therefore clear that the Andean shortening started along the western Andes and subsequently propagated eastward, progressively enlarging the orogen to form the different cordilleras and the Altiplano plateau in between.

Different authors investigated crustal shortening and thickening at ~20–22°S at the scale of the whole Andean mountain-belt. From these earlier studies, total crustal shortening is estimated to ~360 km (e.g., Anderson et al., 2017; Barnes & Ehlers, 2009; Elger et al., 2005; Kley & Monaldi, 1998; McQuarrie et al., 2005; Sheffels, 1990). This crustal shortening contributed to crustal thickening. With a crustal thickness of ~70–80 km (e.g., Heit et al., 2007; Tassara et al., 2006; Wölbern et al., 2009; Yuan et al., 2000; Zandt et al., 1994) beneath the Western Cordillera, the Altiplano and the Eastern Cordillera at these latitudes, the crust is over-

158 thickened compared to the ~45 km thick crust of the South America craton (e.g., Wölbern et al.,
159 2009).

160 2.2 Geological setting of the Western flank of the Andes at ~20–22°S

161 The Andean western flank is formed of three tectono-stratigraphic units at ~20–22°S,
162 aside from the present-day volcanic arc. Starting from the East (oldest and deepest units, exposed
163 at high altitudes) to the West (youngest units, lower altitudes), these are (Figure 1): (1) Andean
164 basement consisting of metamorphic rocks of Precambrian and Paleozoic ages; (2) volcano-
165 sedimentary deposits of Mesozoic age (Triassic–Cretaceous), folded and deformed in a FTB, and
166 (3) unconformably overlain by less-deformed mid-upper Cenozoic (Oligocene – Quaternary)
167 volcanics and sedimentary cover. Magmatic intrusions locally alter these different units, and are
168 mostly Cenozoic (SERNAGEOMIN, 2003).

169 The pre-Andean basement rocks formed during the Late Proterozoic and Palaeozoic,
170 when the Amazonian craton was progressively assembled from various terranes (e.g., Charrier et
171 al., 2007; Lucassen et al., 2000; Ramos, 1988; Rapela et al., 1998). At the end of this period of
172 subduction and continental accretion, intensive magmatic activity (volcanism and major granite
173 intrusions) welded together the basement during the Late Carboniferous to Early Permian
174 (Charrier et al., 2007; Ramos, 2008; Vergara & Thomas, 1984).

175 The Mesozoic deposits (Triassic to Cretaceous), found today along the west Andean
176 flank, formed in a proto-Andean arc and backarc basin system during the early period of the
177 Andean cycle (e.g., Charrier et al., 2007; Mpodozis & Ramos, 1989). Marine and continental
178 sediments are interbedded with volcano-magmatic rocks (Aguilef et al., 2019; SERNAGEOMIN,
179 2003). These Mesozoic units attain locally thicknesses up to ≥10 km (e.g., Buchelt & Tellez,
180 1988; Charrier et al., 2007; Mpodozis & Ramos, 1989).

181 A regional erosional surface called the Choja Pediplain (Galli-Olivier, 1967) developed
182 during the Eocene to Early Oligocene (~50–30 Ma) (e.g., Armijo et al., 2015; Victor et al.,
183 2004). Above this angular unconformity, the up to ~1600 m thick (Labbe, 2019) Cenozoic
184 deposits of the Altos de Pica Formation (Galli & Dingman, 1962) are composed of continental
185 clastic sediments, interbedded with volcanic layers (Victor et al., 2004). The oldest documented
186 age within the Altos de Pica Formation is of ~24–26 Ma from dated ignimbrites (Farías et al.,
187 2005; Victor et al., 2004). From there, an age of ~27–29 Ma for the base of the Altos de Pica

Formation is inferred regionally when extrapolated to the basal erosional surface using an average sedimentation rate. The youngest ignimbrites within the Altos de Pica Formation are dated at ~14–17 Ma (Middle Miocene) (Vergara & Thomas, 1984; Victor et al., 2004). Based thereon and in addition to other younger dated ignimbrites (Baker, 1977; Vergara & Thomas, 1984), Victor et al. (2004) deduced from stratigraphic correlations that the development of the Altos de Pica Formation finished by ~5–7 Ma (Late Miocene) at ~20–22ºS.

Using apatite fission track dating, Maksaev and Zentilli (1999) proposed significant basement exhumation between 50 Ma and 30 Ma, possibly related to basement overthrusting. At ~21°30'S, the geological map of Skarmenta and Marinovic (1981) indicates a west-vergent thrust bringing Paleozoic basement over folded Mesozoic units. Such a thrust contact would imply significant crustal shortening across the western Andean margin, yet to be further documented in the field and quantified. In the folded sedimentary series further west, Victor et al. (2004) determined ~3 km of shortening recorded by the Cenozoic deposits of the Altos de Pica Formation, i.e. accumulated between ~29 Ma and ~5–10 Ma. However, these authors did not take into account the deformation of the underlying, more deformed Mesozoic units. Haschke and Günther (2003) estimated that >9 km of shortening across the western flank in the Sierra Moreno area (~21°45'S) occurred since the Late Cretaceous to Eocene on a west- and east-verging thrust system. It follows that even if published data hint at the existence of a west-verging fault system along the western Andean front at ~20–22°S, its geometry, kinematics and total amount of shortening have not yet been satisfactorily evaluated.

Unconformable mid-upper Cenozoic clastic sediments and ignimbrites hide most often the folded Mesozoic layers and their contact with the basement. Investigation is thus limited to sparse areas of few tens of km of extent, only where the interplay of erosion, canyon incision and exhumation has removed this Cenozoic cover and allows for structural observations (Aguilef et al., 2019; SERNAGEOMIN, 2003) (Figure 1). In this study, we focus on two relatively accessible outcrop sites: (1) At ~21°30'S, where the Paleozoic basement thrusts over the Mesozoic according to Skarmenta and Marinovic (1981). This zone will be referred to as the Pinchal area (next to Cerro Pinchal, 4193 m a.s.l.) (box A on Figure 1). (2) At ~20°45'S, where the FTB composed of deformed Mesozoic units has been significantly eroded and allows observations. This zone is hereafter named Quebrada Blanca area, after its largest canyon (box B on Figure 1).

3. Data and Methods

3.1 Available Data

The most detailed existing geological map for the Pinchal area is the Quillagua map (1:250,000 scale, Skarmenta & Marinovic, 1981), which only provides very large-scale information but hints for the existence of a major basement thrust. For the Quebrada Blanca area, the recent Guatacondo map (1:100,000 scale, Blanco & Tomlinson, 2013) provides detailed and updated information on the stratigraphy and structure. There, the folded Mesozoic rocks are well exposed on a relatively wide area (~15 km east–west extent) and their structure has been preliminarily mapped and qualitatively described by Blanco and Tomlinson (2013) and Armijo et al. (2015).

Enhanced cartographic details can be deduced from high-resolution satellite imagery. We use Google Earth imagery (Landsat 7, DigitalGlobe) whose resolution varies from a few meters to a few tens of meters depending on the zones. In addition, this work benefits from very high-resolution imagery from the European Pléiades satellites. Using the MicMac software suite (Rosu et al., 2014; Rupnik et al., 2016), we calculate high-resolution DEMs from tri-stereo Pléiades imagery, with a 0.5 m resolution. These DEMs are down-sampled to a resolution of 2 m to enhance data treatment and calculations (e.g., stratigraphic projection and image processing). Relative vertical accuracy may reach ~1 m, depending on local slope.

Field observations acquired during two field surveys in March 2018 and January 2019 complete the dataset and permit the verification of the large-scale data acquired from maps and satellite imagery. Difficult accessibility and field logistics in the remote and desert Pinchal area only allow detailed field observations on a relatively limited area. Observation points and the off-road track followed to reach our field site in the Pinchal area are provided as supplementary material.

3.2 Establishing structural maps

We establish structural maps for the two investigated sites. We use an approach based on the 3D-mapping of stratigraphic layers on satellite imagery (Armijo et al., 2010; Riesner et al., 2017). More precisely, layers are traced and correlated on Google Earth satellite images. The so-obtained georeferenced traces are projected on the DEM-derived topographic map, and

compared with geological maps, mainly for stratigraphic and age references. Field observations allow ground verifications and provide supplementary details, such as the existence of minor thrusts and folds, the observation of polarity criteria or the local measurement of dip angles.

The approach used here is mainly limited by local geological complications. Continuous mapping of Mesozoic strata is indeed locally complicated where incision of Cenozoic strata is limited, where magmatic intrusions and associated hydrothermalism alter the surrounding structural geometries, where soft layers with no well-expressed bedding such as marls are present (ex: Pinchal area), or where small landslides or recent sediment deposits hide the underlying deformation pattern. Therefore, geometrical observations and detailed mapping of the structures may be locally difficult, in some zones impossible. These difficulties cause uncertainties in precisely correlating mapped layers and may result in metric to decametric errors (if correlating a layer with its neighbor by error) but do not modify our large-scale (km) results and interpretations.

3.3 Building structural cross-sections

We use structural measurements, field observations and the obtained structural map to build cross-sections of the two investigated areas.

In the Pinchal area – because of limited canyon incision, marls, and frequent blanketing of the structures by Cenozoic cover – we build our structural cross-sections mainly from field observations (strike and dip angles, polarity criteria, first-order stratigraphic column), with additional information taken from satellite imagery.

In contrast, in the Quebrada Blanca area, we mostly build our subsurface cross-section from mapping on satellite imagery. Here, we follow the approach already proposed in Armijo et al. (2010) and described in detail in Riesner et al. (2017). The mapped georeferenced horizons are projected on the high-resolution Pléiades DEMs. Using a 3D-modeler, the horizons can be visualized interactively. In order to precisely assess the local average dip and strike angles of deformed Mesozoic layers, we project these layers along swath profiles chosen where Mesozoic strata crop out the best, where folds are mostly cylindrical and where incision (and therefore topographic relief) is most significant. It should be noticed that river incision is here significantly lower (a few hundred meters at most) than at the latitude of Santiago de Chile (~33°30’S) where this approach has been previously employed (Riesner et al., 2018, 2017). In any case, we

successfully obtain the overall sectional geometry of layers, and by comparing with the structural map, we determine the approximate locations of the major synclinal and anticlinal fold axes. By respecting the classical structural rule of constant layer thickness, we derive fold geometries.

The limits of our interpretations mostly relate to the difficulty of unambiguously correlating stratigraphic layers, and to the fact that, in reality, layers may not always keep constant thicknesses. As incision and local topographic relief are reduced to a few hundred meters at most, the construction of cross-sections is mostly restricted to extrapolating surface dip angles at depth.

3.4 Crustal shortening and kinematic modeling

We use the obtained subsurface cross-sections to estimate the minimum fold-related shortening across the investigated sites, employing a simple line-length-balancing approach. However, as this approach does not allow for quantifying the shortening absorbed by thrusting, we additionally model deduced anticlinal geometries using a numerical trishear approach (e.g., Allmendinger, 1998; Erslev, 1991). We use the code FaultFold Forward (version 6) (Allmendinger, 1998) in order to jointly model thrust displacement and anticlinal folding. Trishear models the deformation distributed within a triangular zone located at the tip of a propagating fault. This forward modeling relies on a set of parameters that are here adjusted by trial and error to fit structural geometries. By adding sedimentary layers at various steps during ongoing deformation, we model syntectonic deposition and subsequent deformation, in order to reproduce deformation of Cenozoic layers. Additional information on trishear modeling, together with the range of tested parameters, are provided in supplementary material. We recognize that our best-fit model parameters may not be unique. This is not expected to impact much estimated total shortening as this result depends mostly on final cross-sections. This point will be further discussed in section 7.3 and in the supporting information.

4. Basement thrust and deformed Mesozoic series within the Pinchal area (~21°30'S)

4.1 Synopsis of the previous structural interpretation

In the Pinchal area, the Quillagua 1:250,000 geological map (Skarmenta & Marinovic, 1981) reports a thrust contact between the Paleozoic basement and the folded Mesozoic series of

306 the Quinchamale formation to the west. These Mesozoic deposits, formed supposedly in a
307 backarc basin context, would be of Jurassic age and would contain two sub-units. Skarmeta and
308 Marinovic (1981) propose that the core of the folded Mesozoic series is Oxfordian (~157–163
309 Ma) with younger Kimmeridgian (~152–157 Ma) layers east and west of it. The mapped
310 structure is therefore an anticline, with an east-dipping axial plane.

311 Our observations confirm the existence of a major basement thrust in the Pinchal area.
312 However, our field investigations disagree with the structural interpretation of the folded
313 Mesozoic series proposed by Skarmeta and Marinovic (1981) just west of the basement thrust.
314 Even though we do not know the absolute ages of the sedimentary series, our structural
315 observations and the relative stratigraphic ages of Mesozoic units, as deduced from either
316 structural or sedimentary polarity criteria, suggest a synclinal structure rather than an anticlinal
317 one.

318 Hereafter, we describe our own stratigraphic and structural observations and
319 subsequently present our interpretation of the Pinchal area.

320 ## 4.2 Field observations

321 ### 4.2.1 Stratigraphic observations

322 In the absence of an existing detailed local stratigraphic documentation, we propose a
323 first-order stratigraphic column from our structural, stratigraphic and sedimentary field
324 observations. In the landscape, the three main tectono-stratigraphic units are clearly
325 distinguishable (Figure 2): (1) the metamorphic basement, (2) the continuous Mesozoic
326 sedimentary series (with a continuum from continental to marine facies) and (3) the continental
327 Cenozoic cover. The first-order stratigraphic column (Figure 3) is hereafter described from the
328 oldest to the youngest units. Detailed field pictures of identified and individualized sedimentary
329 formations are provided in supplementary material to complement the forthcoming stratigraphic
330 descriptions.

331 The Paleozoic basement (Figure S1) dominates the eastern part of the Pinchal area, and is
332 composed of mainly coarse-grain granodiorites and diorites, as well as metamorphic rocks
333 comprising gneisses, migmatites and mica-schist, consistent with documented characteristics of
334 the basement in the area (Skarmenta & Marinovic, 1981).

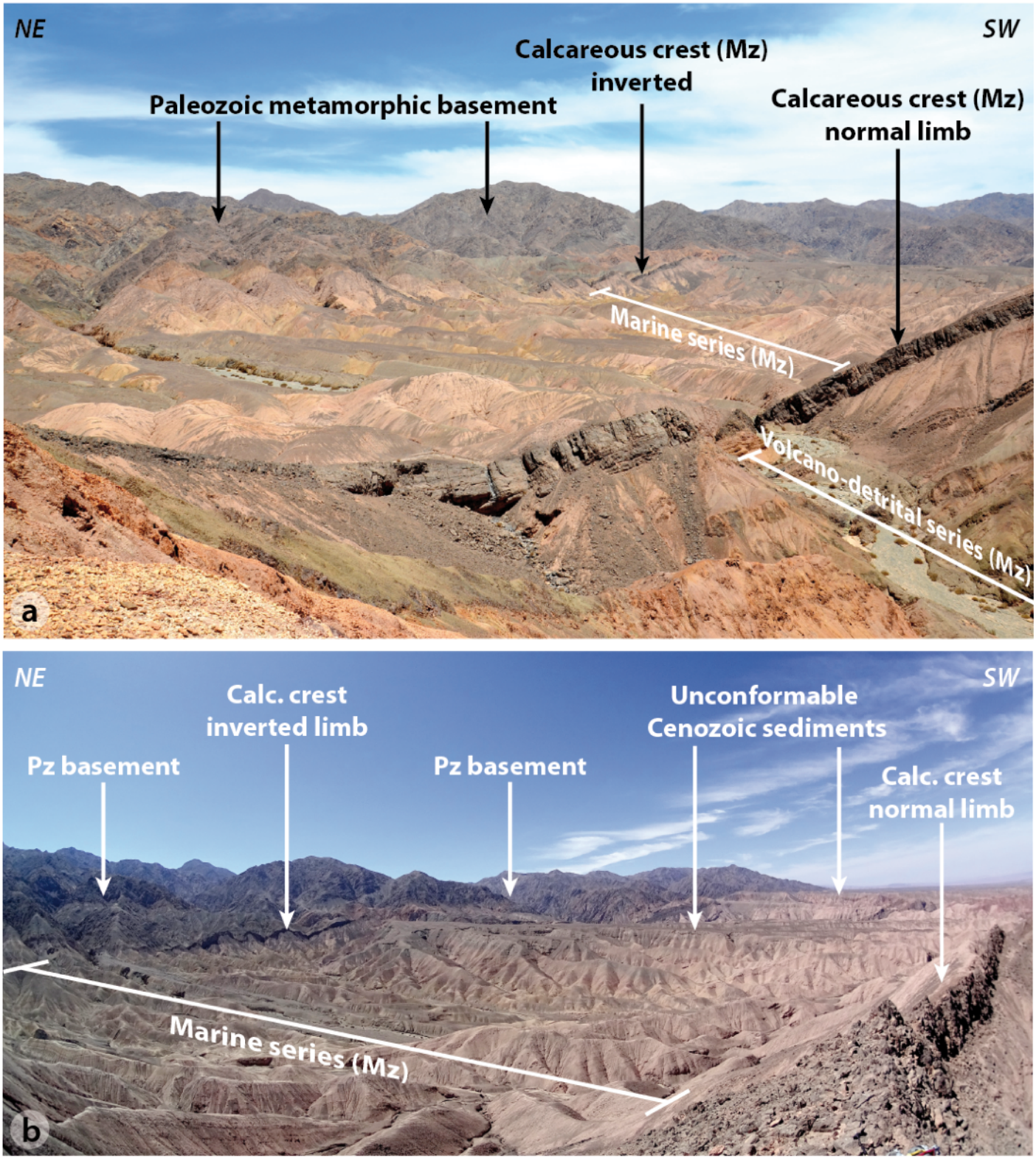

Figure 2. Landscape field overviews of the Pinchal area depicting the main tectono-stratigraphic units. The Paleozoic (Pz) basement stands clearly out in the background, characterized by its darker color and higher altitudes. The Mesozoic (Mz) series in the central part and in the foreground bear a marine part and a volcano-detrital part, delimited by an outstanding calcareous (Calc.) crest. Unconformable Cenozoic erosional surfaces, with limited fluvial deposits can also be observed. View points of both pictures are located on Figure 4.

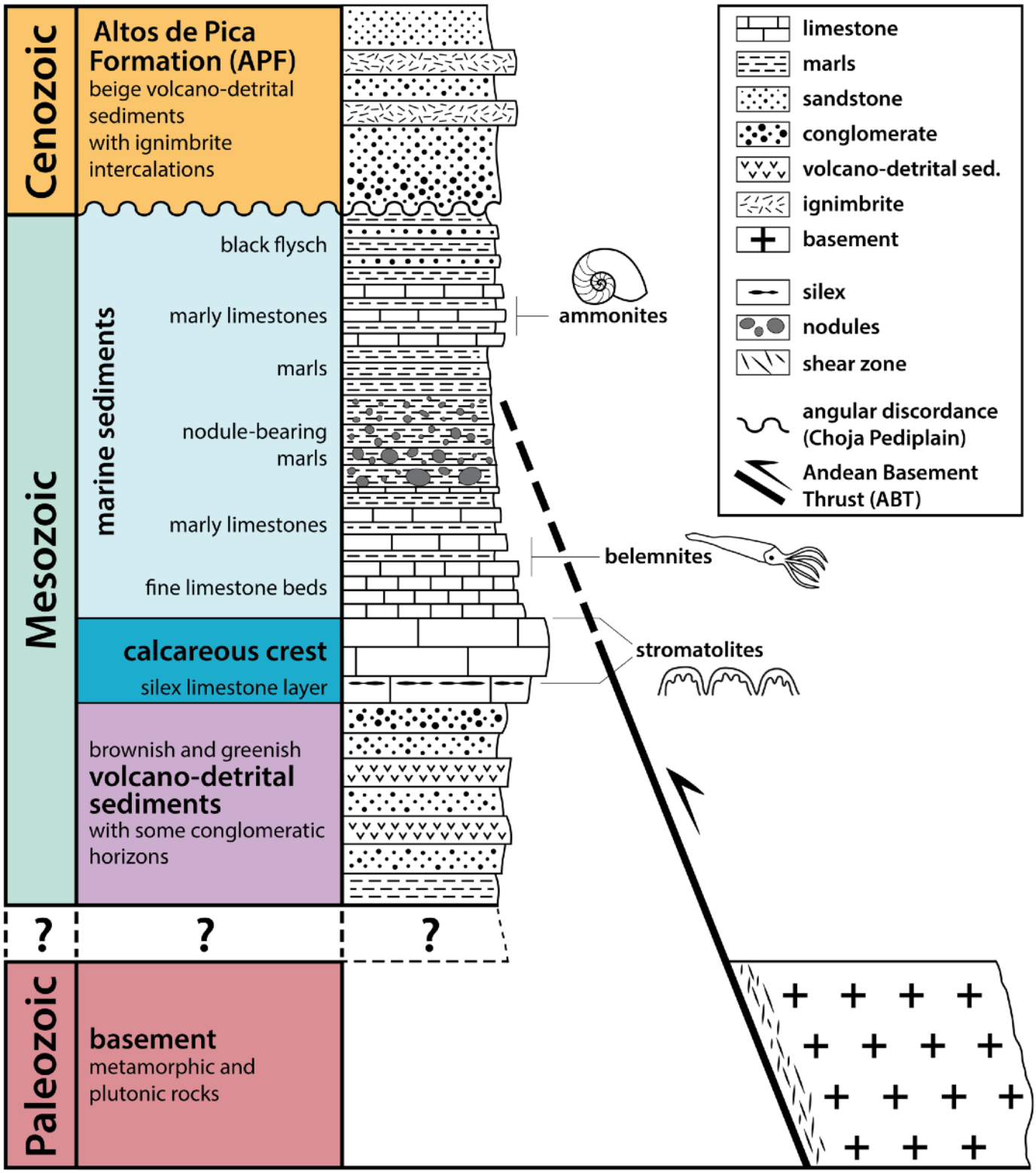

Figure 3. First-order stratigraphic column of the Pinchal area derived from field observations obtained mainly along Quebrada Tania (Figures 4 and 5a) where the Mesozoic series seems to be most complete. By analogy to regional descriptions, these layers are suspected to be Triassic at the base, and Jurassic in the case of the marine fossiliferous levels (see section 4.2.1 for additional details). The description of Cenozoic units is here completed based on the work of Victor et al. (2004). Color-code in line with maps (Figures 1, 4 and S13) and cross-sections (Figure 5). In the Pinchal area, Paleozoic basement overthrusts folded Mesozoic series along the Andean Basement Thrust (ABT), so that part of the deeper and older Mesozoic series may be missing here (as depicted by "?"). Abbreviation "sed." for sediments. See Figures S1–S12 and corresponding captions (in supplementary material) for detailed sedimentologic descriptions.

335 The older part of the outcropping Mesozoic series consists of continental deposits, with a
336 high content of Paleozoic lithics and volcano-clastic and tuffitic low-rounded conglomerates, of
337 greenish, beige and brownish colors, and clast-sizes varying from a few millimeters to few
338 decimeters (Figure S2). At places, these rocks bear sedimentary polarity criteria such as grain-
339 grading, grain-sorting, cross-bedding and tangential beds (Figure S3). In the eastern part of the
340 Pinchal area, we locally observed below this series some dark green detrital pelites (lutites)
341 (Figure S4). On the basis of petrographic and sedimentological correlations, these detrital
342 Mesozoic sediments resemble to units mapped as Triassic north of the Pinchal zone (between
343 21º–21º30'S) in the Quehuita area (Aguilef et al., 2019).
344 In paraconformity, a characteristic limestone layer marks the beginning of a marine
345 sequence within the Mesozoic series, evidencing a marine transgression process. We hereafter
346 refer to this layer as the "calcareous crest" as it is prominent in the landscape (Figure 2) and as
347 such can be easily used as a reference marker in the field or in satellite images. The base of the
348 calcareous crest is characterized by the presence of silex layers or nodules (Figure S5).
349 Upsection, numerous stromatolites (Figure S6) and bivalves (Figure S7) are found within the
350 unit. Its thickness varies between a few meters (less than 10 m) in the eastern part, to ~10–20 m
351 to the west.
352 The calcareous crest is overlain by thin-bedded (cm–dm) limestone layers of rose-beige
353 color (Figure S8), over a thickness of ~50–100 m. Going upsection, the marine series becomes
354 progressively more marly, limestone layers become more rare and the color more beige,
355 evidencing a deeper marine paleo-environment bearing fossiliferous marl layers. Belemnite
356 fossils were encountered in the lower part of this limestone-to-marl sequence. Characteristic
357 calcareous oval concretions of variable diameter (cm to m) (Figure S9), are pervasive at the
358 transition from marly limestones to marls. The marls bear ammonite fossils, which we have not
359 identified. These Ammonite species could be Perisphinctes, Euaspidoceras, Mirosphinctes and
360 Gregoryceras, according to the notice of the Quillagua geological map (Skarmenta & Marinovic,
361 1981) if applicable here. In this case they would be associated with a Middle Jurassic age
362 (Bajocian to Callovian). The series from the thin-bedded limestones to the top of the beige marls
363 is ~200 m thick, along one of the canyons and sections investigated in the field (Quebrada
364 Tania).

Upsection, the beige marls become progressively more calcareous again, with the presence of thin limestone layers (Figure S10). Finally, this marine sequence ends with black marls containing layers of beige sandstones (mm to few cm – rarely dm – thick) (Figure S11), indicative of a detrital component in a probable deep seated basin, comparable to the "flysch" series in the Alpine basins (Homewood & Lateltin, 1988). This unit is hereafter called "black flysch", and has a minimum thickness of ~50 m.

Continental-clastic Cenozoic deposits (Altos de Pica Formation), unconformably overlie the folded Mesozoic series over the Choja erosional surface (Galli & Dingman, 1962; Galli-Olivier, 1967; Victor et al., 2004), evidencing a regression process (Figures 2 and 3). They are mainly composed of alluvial fan facies that were sourced from the mountain front immediately to the east, with different aggradational terraces. Locally, ignimbrites are observed to cover these clastic series. We encountered red arenites at the base of the Cenozoic series in the western part of the Pinchal area (Figure S12). The age of the oldest sedimentary deposits above this erosional surface is regionally inferred to be ~27–29 Ma (Victor et al., 2004; see also section 2.2).

4.2.2 Structural Observations

The structural map of Figure 4 illustrates the main stratigraphic and structural features observed in the field and by mapping on satellite imagery. Two ~east–west cross-sections show detailed surface observations along two accessible representative canyons: Quebrada Tania and Quebrada Martine (Figure 5a,b). The Quebrada Tambillo incises deeper into folded units, and as such surface structural observations can be further extrapolated at depth (Figure 5c).

The easternmost part of our study area is marked by a major west-vergent thrust bringing the metamorphic basement over the Mesozoic units. This basement thrust is hereafter named the Andean Basement Thrust (ABT). The west-vergent thrust-nature of the shear zone between the Paleozoic basement and the Mesozoic units is observable in the field (Figures 2 and 6). The characteristic C/S-fabric ("Cisaillement/Schistosité") – underlines the penetrative shearing of the basement rocks within and nearby the thrust shear zone, and indicates a top-to-the-west thrusting direction (Figure 7a). The ABT roughly follows a north–south direction (Figure 4). This major contact often resumes to a single basement thrust (Figure 5a,c), but may also show local geometrical complexities, with secondary thrusts and branches, eventually involving basement with stripes of trapped Mesozoic units, as for example along Quebrada Martine (Figure 5b).

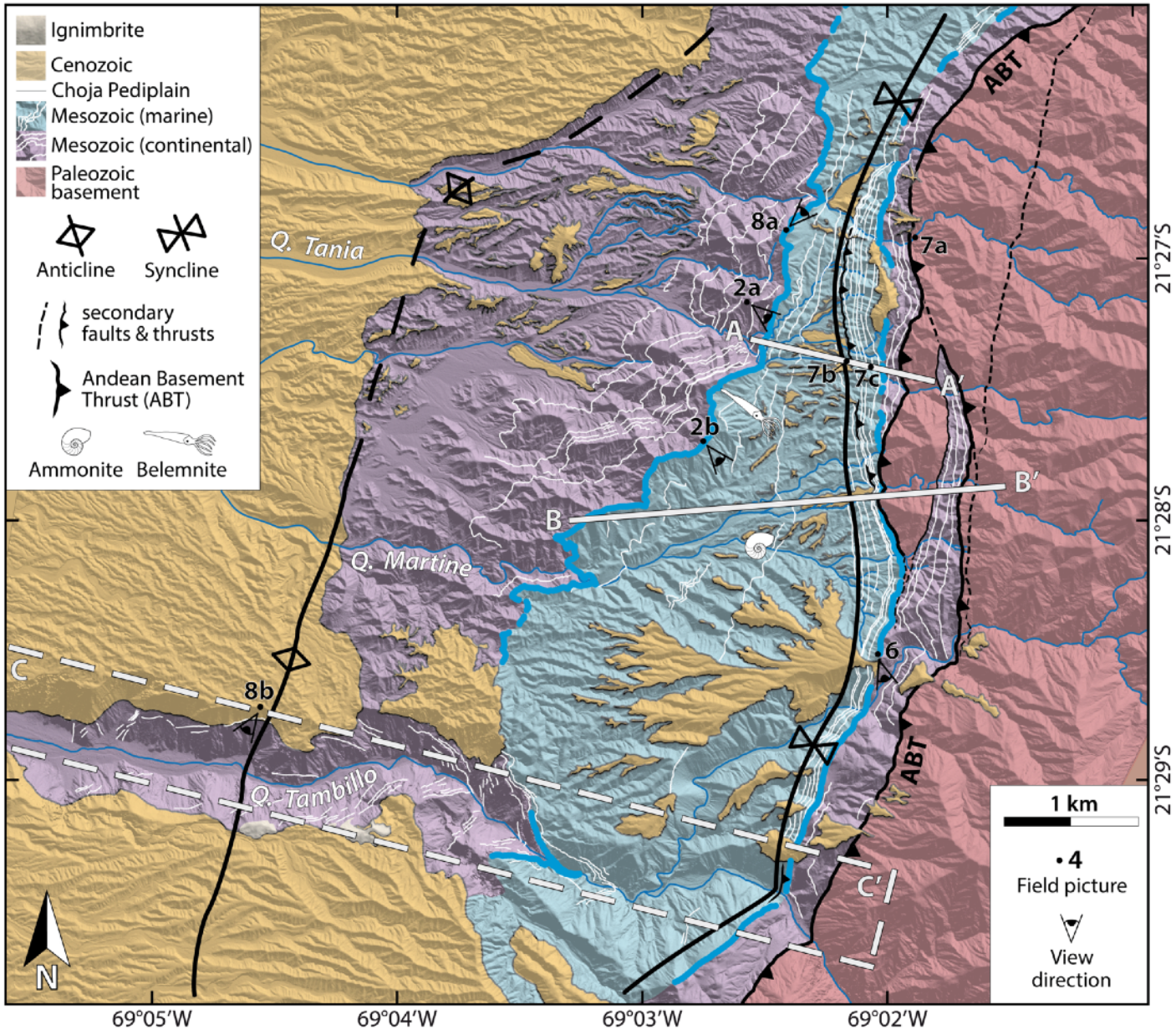

Figure 4. Structural map of the Pinchal area (at ~21°30'S) derived from mapping in the field and on satellite imagery (location on Figure 1, box A). White thin lines highlight Mesozoic layers mappable on satellite images. Thick blue line depicts a robust, out-sticking Mesozoic limestone layer forming a prominent calcareous crest in the landscape (Figure 2). A–A' and B–B' sections locate the topographic profiles used for the surface cross-sections of Quebrada Tania and Quebrada Martine, respectively (Figures 5a-b). In the case of the Quebrada Tambillo cross-section, a topographic swath profile was used along C–C'. The fold axes are relatively well defined for the synclinal fold, but less well constrained for the anticlinal fold because only observable along Quebrada Tambillo. Black dots refer to the location of field photographs, and are numbered according to the figures where these pictures are reported.

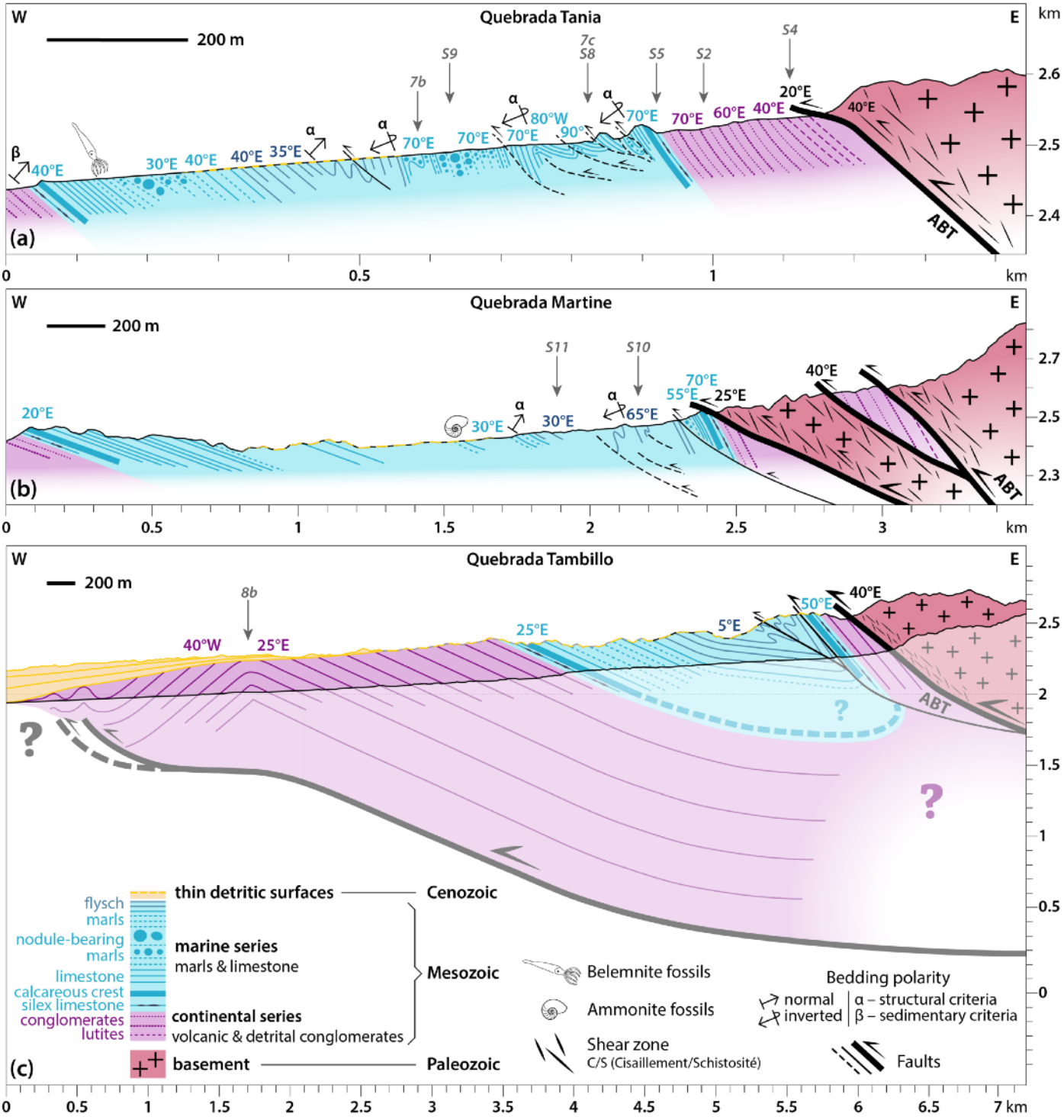

Figure 5. Surface field observations and cross-sections along **(a)** the Quebrada Tania (A–A' on Figure 4), **(b)** the Quebrada Martine (B–B' on Figure 4), and **(c)** the Quebrada Tambillo (C–C' on Figure 4). Reported dip angles have been measured in the field. Faults are outlined in black, and dashed when they are only observable at a local spatial scale. Only larger faults (continuous lines) are mapped on Figure 4. Grey numbers with arrows point out to field pictures and indicate the associated figure. In the case of the Quebrada Tania section **(a)**, the sedimentary polarity criterion (β) indicated to the West of the section has been observed ~1 km further downstream than reported here. For the Quebrada Martine section **(b),** note the stripe of continental Mesozoic rocks trapped in between two strands of the Andean Basement Thrust (ABT). Sub-surface interpretation from surface observations is reported with transparent colors in the case of the Quebrada Tambillo section **(c)**. Note the different spatial scales of the three sections.

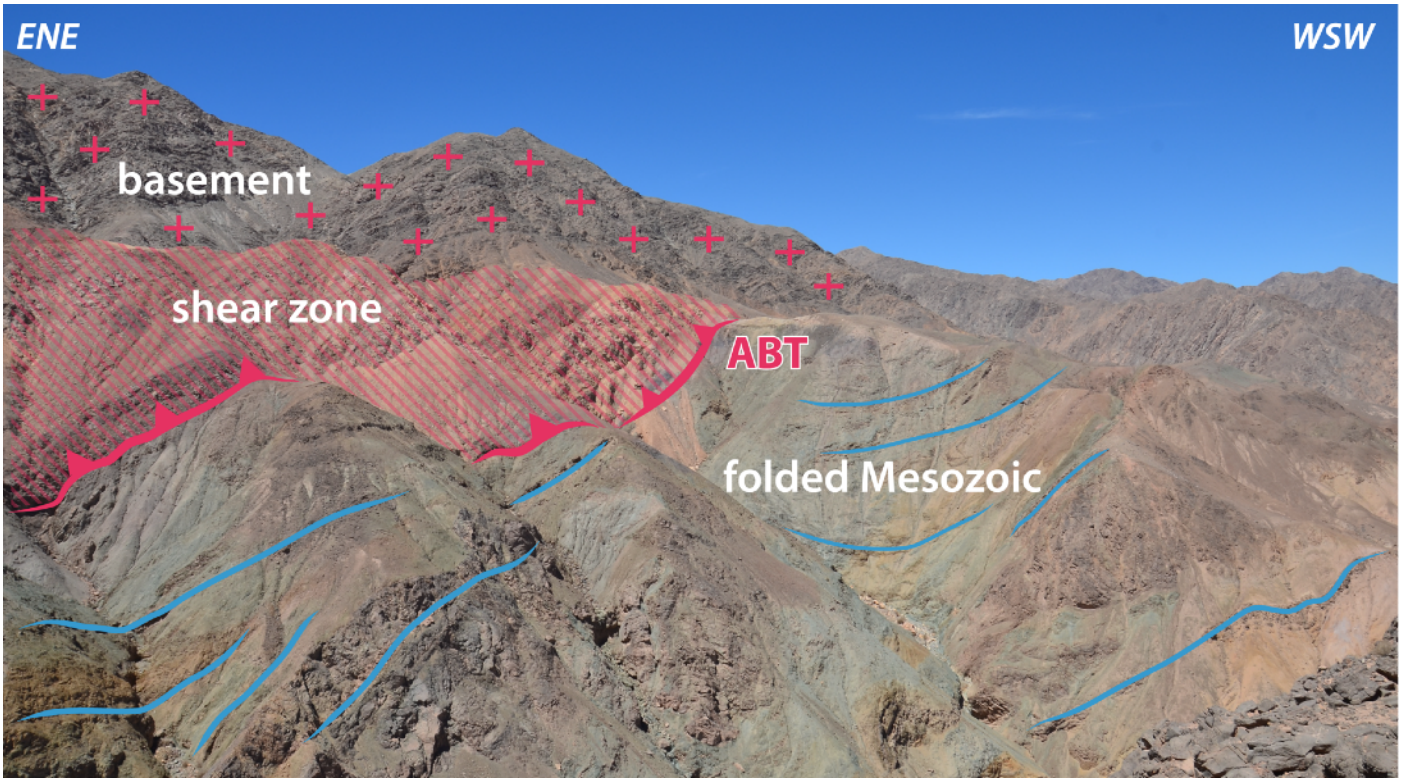

Figure 6. Field view of the Andean Basement Thrust (ABT), overthrusting the dark-grayish Paleozoic basement over the greenish folded Mesozoic units. Reddish rocks on the hanging wall to the East-Northeast correspond to the thrust shear zone (hatched area in picture). Location on Figure 4. Non-interpreted photograph can be found in the supporting information (Figure S15).

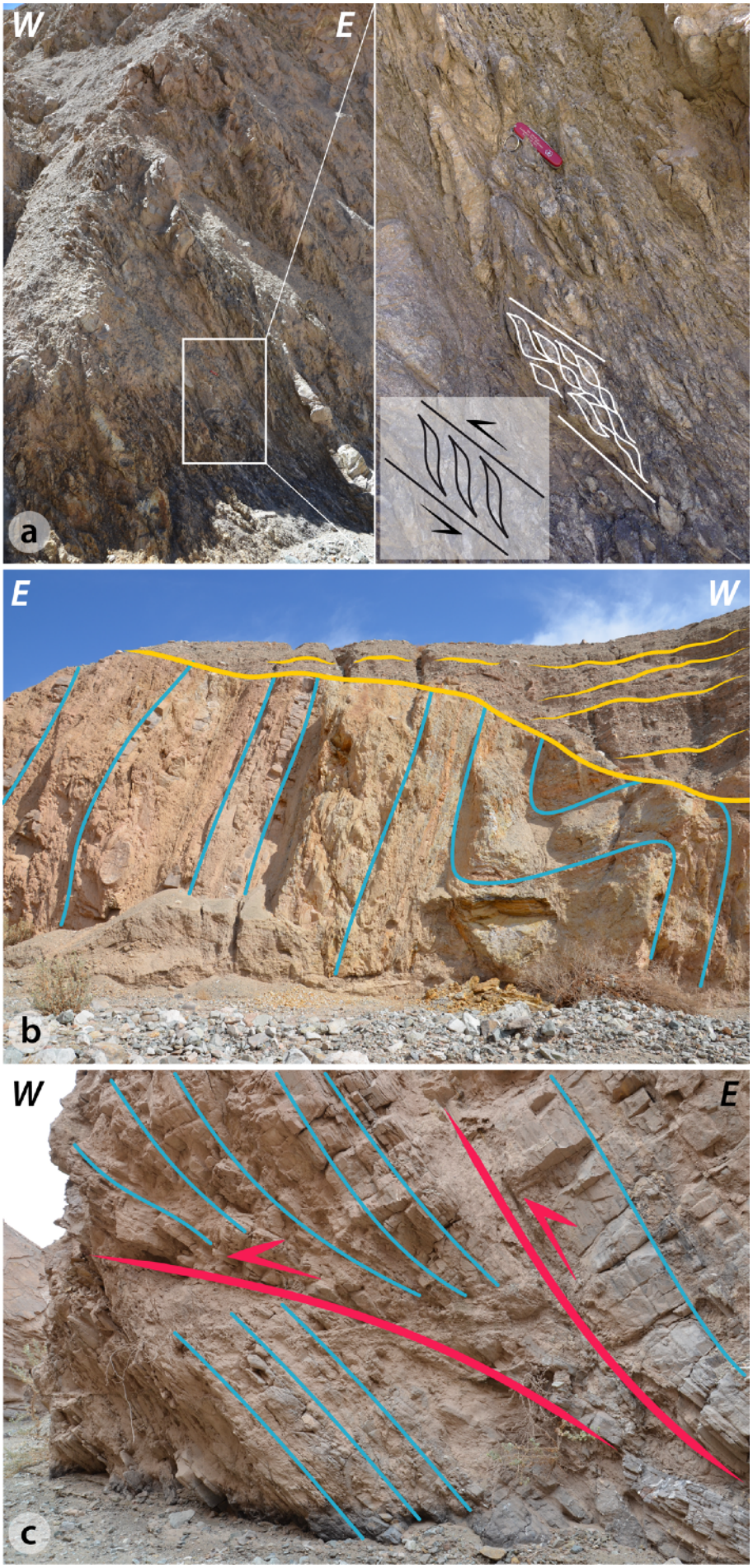

Figure 7. Field pictures of small-scale structural features characteristic of the deformation within the Pinchal area (Location on Figures 4 and 5). Non-interpreted photographs for (b) and (c) can be found in the supporting information (Figures S16).

(a) Shear band with characteristic C/S-fabric (for "Cisaillement/ Schistosité") indicative of top-to-the-west thrusting. Observation within the metamorphic basement in the hanging wall of the Andean Basement Thrust.

(b) Example of a small-scale fold within the marine Mesozoic units (blue line) in Quebrada Tania, within the inverted limb of the mapped syncline, nearby the fold axis. Note also the erosional surface (yellow) forming the unconformable contact between the Cenozoic deposits over the deformed Mesozoic.

(c) Small-scale thrusts (steep red line to the right) and décollements (flat red line to the left) observed within the marine Mesozoic strata (blue) of the inverted synclinal limb along Quebrada Tania. The limestone-dominated cm–dm beds are characteristic of the upper part of the marine Mesozoic units (Figure 3).

West of the ABT, a FTB consisting of folded Mesozoic units is observable (Figures 2 and 4). From east to west, this west-vergent FTB is first formed of an asymmetric and overturned syncline (Figure 8a), followed by a relatively symmetric anticline (Figure 8b). The eastern limb of the syncline, right beneath the ABT, is inverted and locally highly faulted and folded (Figures 5 and 7b-c). Within this inverted limb, the series goes westward (and upsection) from sheared lutites beneath the ABT followed by Mesozoic detrital series with conglomerates, to the Mesozoic marine series from the calcareous crest upsection to the marly limestones. The overturned strata are steeply dipping (50–70ºE). Penetrative small-scale deformation can be observed pervasively within the marine Mesozoic series, in the form of numerous local small folds, kinematically indicative of an inverted fold limb (Figure 7b), and local secondary shear zones and thrusts (Figure 7c).

Going westward, as observed in detail along Quebrada Tania (Figure 5a), the eastern part of the black flysch bears small-scale folds characteristic of the inverted fold limb, whereas normal limb folds are observed slightly further west: the axis of the overturned west-vergent syncline therefore passes through the black flysch. Part of the Mesozoic series is missing, as overthrusting within the flysch and (marly) limestones is observed frequently along Quebrada Tania (Figure 5a). The overturned syncline is therefore found to be broken by a secondary thrust fault striking approximately parallel to the ABT and roughly coinciding with the synclinal fold axis (Figures 4-5). Westward, the normal western limb of the syncline encompasses the whole Mesozoic series from the black flysch down-section to the Mesozoic volcano-detrital series, with more gentle dip angles (20–40ºE) (Figures 2 and 5). Penetrative deformation is observed to be limited here.

The continental Mesozoic layers of the normal limb of the syncline flatten toward the west. The section along Quebrada Tambillo (Figure 5c) shows a broad, overall symmetrical, anticlinal fold (Figure 8b). Its fold axial plane is steep, dipping ~80°E. The western flank of this large anticline is marked by smaller, secondary folds with westward decreasing wavelength and amplitude. Field logistics did not permit further detailed structural observations within this anticline.

The Mesozoic sediments immediately west of the basement are unconformably covered by sheet-like, river-incised Cenozoic fluvial deposits, forming aggradational terraces unconformably deposited above erosional surfaces at different elevations, of varying extension

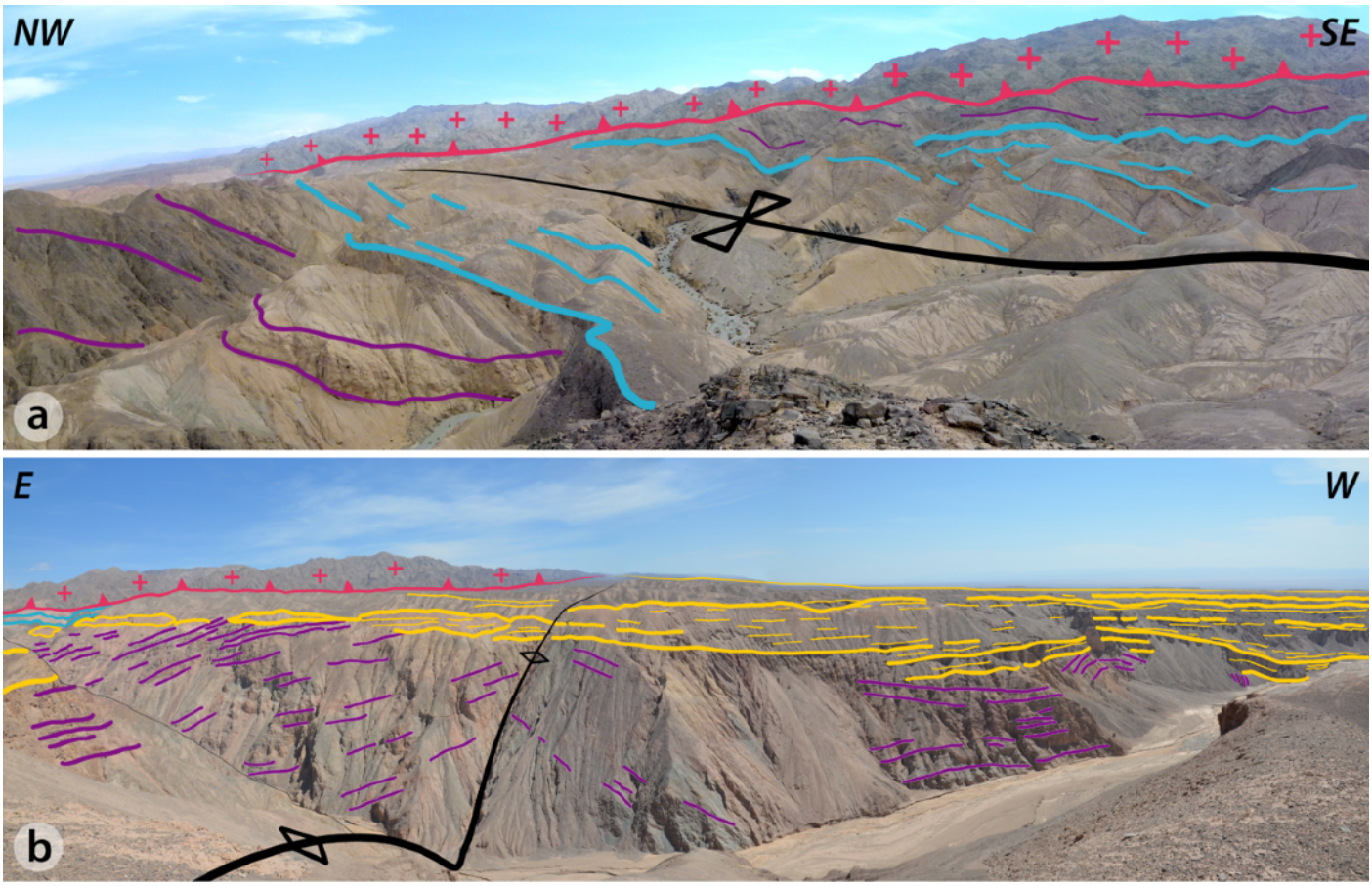

Figure 8. Field pictures of the two major folds within the Pinchal area (location on Figure 4). Non-interpreted photos can be found in the supporting information (Figures S17).

(a) Panoramic view on the north-eastern part of the Pinchal area. The Paleozoic basement (red crosses) overthrusts the Mesozoic units (blue and violet horizons) along Andean Basement Thrust (ABT - red line with triangles). The topographic low locates the synclinal fold axis. The calcareous crest on both sides is highlighted by the thick blue lines. For better visibility, Cenozoic erosional surfaces covered by thin deposits are not highlighted.

(b) Panoramic view along Quebrada Tambillo, in the southern part of the Pinchal area. The ~200 m deep incised canyon reveals the geometry of the large western anticline affecting Mesozoic layers (violet) underneath the unconformable Cenozoic strata (yellow). The fold axis (black line) probably coincides with an approximately vertical fault, also well observable on satellite imagery. Note also the repetition of smaller folds with westward decreasing amplitude and wavelength discernable beneath the westward thickening Cenozoic growth strata to the right of the picture. The Mesozoic calcareous crest (blue) and the Paleozoic basement (red crosses) over the ABT (red) appear in the far eastern background.

and of probably different ages (Figure 2b). The majority of these erosional surfaces shows a westward tilt (Figure 5c). Further west, the Cenozoic deposits become thicker and bury the westward extent of the fold-and-thrust-belt. Westward thickening of the Cenozoic layers is clearly observable in Quebrada Tambillo and indicates the presence of growth strata at the front of the anticline deforming the Mesozoic series (Figures 5c and 8b).

4.3 Structural Interpretation

The synthetic cross-section of Quebrada Tambillo (Figure 5c) summarizes our interpretation of the sub-surface structural geometry of the Pinchal area. Tectonic shortening in the Pinchal area is thus materialized by the presence of the ABT and by the folded and faulted Mesozoic strata.

Based on the dip angle of the C/S-fabric in the ABT shear-zone (Figure 7a) and on the mapping of the ABT on satellite imagery, we estimate that the ABT has a subsurface dip angle of ~40ºE, even though locally flatter such as along Quebradas Tania and Martine (Figures 5a-b). All secondary strands of the ABT are expected to root at depth onto the main shear-zone. The secondary thrust breaking the core of the syncline is roughly parallel to the ABT (Figure 4) and is probably a frontal splay fault of the basement thrust. It is therefore expected to also connect onto it at depth. A similar reasoning is proposed to all small-scale thrusts and décollements observed within the inverted synclinal limb, in particular along Quebrada Tania.

Considering that the folds west of the ABT develop above underlying thrusts that connect onto a common detachment is a reasonable and classical assumption for FTBs . This detachment is expected to root at least at the base of the outcropping Mesozoic series, or deeper (Figure 5c). Assuming that the layer thickness is constant over our study area, it can be extrapolated that such detachment is located at least 2 km beneath the topographic surface (i.e. at ~0.2 km a.s.l.), or deeper. To the West of our field area, at the front of the anticline, the small-scale folds with westward decreasing wavelength and amplitude (Figure 8b) are interpreted as the possible expression of disharmonic folding within the forelimb of the anticline and/or of a thrust ramping-up toward the sub-surface at the front of the anticline (Figure 5c).

Because of the pervasive presence of small-scale folding and thrusting, in particular within the inverted limb of the overthrusted syncline, our shortening estimate represents a minimum value and is indicative only of the first-order magnitude of the deformation. Using the

simplified first-order cross-section along Quebrada Tambillo (Figure 5c), line-length balancing results in a minimum of ~1 km of shortening across the two folds documented here, from the ABT to the front of the anticline. A significant – but unconstrained – amount of shortening related to the pervasive deformation observed in the field (Figures 5a-b and 7b-c) is to be added. Further, this minimal shortening of 1 km only encompasses folding of Mesozoic units and does not account for thrusting neither on the thrusts of the FTB nor on the ABT. An estimate of the contribution of thrusting within the FTB will be provided below by modeling (section 6.2).

The minimum thickness of the Mesozoic series is ~2.2 km, as estimated from the normal limb of the syncline along the Quebrada Tambillo section. Thus, it can be considered that the strict minimum exhumation of the basement is equally of ~2.2 km. Assuming a 40°E dip angle for the ABT, this yields a strict minimum displacement of ~2.6 km on this thrust, which has to be added to the minimum shortening estimated from the folding of the Mesozoic series.

5. Structure of the folded Mesozoic series within the Quebrada Blanca area (~20°45'S)

5.1 Stratigraphy of the Quebrada Blanca area

The stratigraphy of the western Andean flank at ~20°45'S is well described in the Guatacondo geological map (Blanco & Tomlinson, 2013). Unlike in the Pinchal area, basement rocks do not crop out in the investigated zone nearby the Quebrada Blanca (Figure 9), but larger scale maps (e.g., SERNAGEOMIN, 2003) show Paleozoic basement units further east and higher in the topography (Figure 1).

The Mesozoic units of the Quebrada Blanca are of Jurassic to Cretaceous age (Blanco & Tomlinson, 2013), have been deposited in a back-arc basin context in successive transgression–regression sequences (Charrier et al., 2007), and are subdivided into three formations: (1) The Late Oxfordian Majala Formation, a clastic unit of sandstones, shales and subordinately stromatolitic limestones of transitional marine origin (Blanco et al., 2012; Blanco & Tomlinson, 2013; Galli-Olivier, 1967); (2) the Late Jurassic / Early Cretaceous Chacarilla Formation, a continental (fluvial) clastic sequence (Blanco & Tomlinson, 2013; Dingman & Galli, 1965); and (3) the Late Cretaceous Cerro Empexa Formation, an andesitic volcanic and continental sedimentary unit (Blanco et al., 2000; Blanco & Tomlinson, 2013; Dingman & Galli, 1965). The Majala and Chacarilla Formations are both of reddish and beige colors and predominantly bear

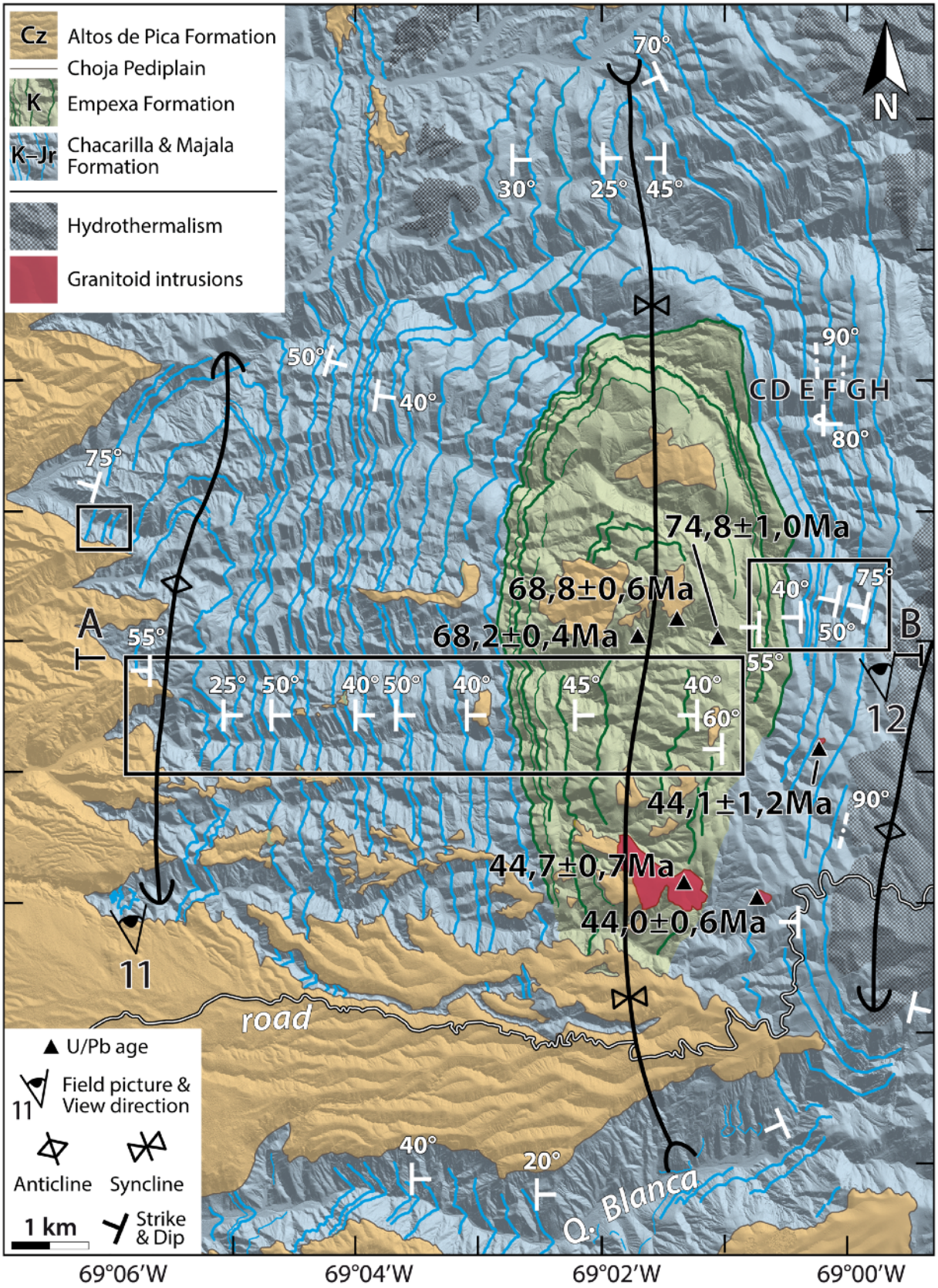

Figure 9. Structural map of the Quebrada Blanca zone (at ~20°45'S), refined from Armijo et al. (2015) (location on Figure 1, box B). Colored lines report mappable layers. For visibility, only major, well-correlated layer traces are represented here. Black boxes locate the swath profiles from which layers were projected for the construction of the structural east–west cross-section (Figure 10). The A–B section corresponds to the topographic profile used for this same cross-section. Strike and dip measurements are extracted from 3D-mapping (see section 3.3) or observed in the field. Strike without dip derives from satellite imagery. Thick black lines correspond to major fold axes. Field pictures are located (with view direction), and numbered according to the associated figure. Ages from uranium-lead (U/Pb) radioisotope dating on zircon are taken from the Guatacondo geological map (Blanco and Tomlinson, 2012). Letters C, D, E, F, G and H to the North-East (within the folded Cretaceous Empexa Formation) report the layers illustrated on Figure 12. Cz: Cenozoic; K: Cretaceous; Jr: Jurassic; Q: Quebrada.

detritic sediments. The Cerro Empexa Formation appears greyish and massive in the field, and its age has been determined from uranium-lead (U/Pb) dating on zircon minerals to ~68–75 Ma (Blanco et al., 2012; Blanco & Tomlinson, 2013; Tomlinson et al., 2015) (Figure 9).

The Cenozoic deposits of the Altos de Pica Formation here also unconformably overlie the Mesozoic series, over the Choja Pediplain angular unconformity (Galli-Olivier, 1967; see also section 2.2). The age of the basal deposits of the Altos de Pica Formation is estimated regionally to ~27–29 Ma (Blanco & Tomlinson, 2013; Victor et al., 2004).

Magmatic intrusions and hydrothermalism occur locally, and hide the eastern continuation of the folded Mesozoic series. Some of these intrusions are dated by uranium-lead (U/Pb) on zircons at ~44 Ma (Blanco & Tomlinson, 2013) (Figure 9).

5.2 Structural observations

The structural map of the Quebrada Blanca area (Figure 9) highlights the main stratigraphic and structural elements observed in the field and by mapping from satellite imagery. Although the cartography of the FTB is complicated by the persistent Cenozoic cover (notably in the west and south), and by magmatic intrusions and hydrothermalism (particularly to the east), three large-scale folds are clearly observable: a wide syncline in the center, bounded by two anticlines to the east and west. The scale of these major folds is multi-kilometric (Figure 9). The cross-section of Figure 10 illustrates the asymmetry of the folds. Both anticlinal folds have steeper western limbs (dip angles vary mostly between ~50–80ºW), whereas their eastern limbs have more gentle dip angles (varying mostly between ~20–50ºW) (Figure 10a). It should be noted that the eastern flank of the eastern anticline is widely hidden by magmatic intrusions and hydrothermalism. The central syncline is wider and more symmetric, with dip angles of ~40–50° on both limbs. The anticlines involve the Majala and Chacarilla Formations, while the core of the syncline bears the Cerro Empexa Formation. Overall, the folded series – and in particular the anticlines – document a clear west-vergence of the FTB (Figure 10c). From our projection of the strata mapped on satellite imagery, the Mesozoic series are observed to be concordant (Figures 10a-b). The cross-section of the Guatacondo map (Blanco & Tomlinson, 2013) proposes an angular unconformity between the Jurassic and Cretaceous units, however not observed here from our large-scale mapping. As this unconformity does not produce any evident change in the

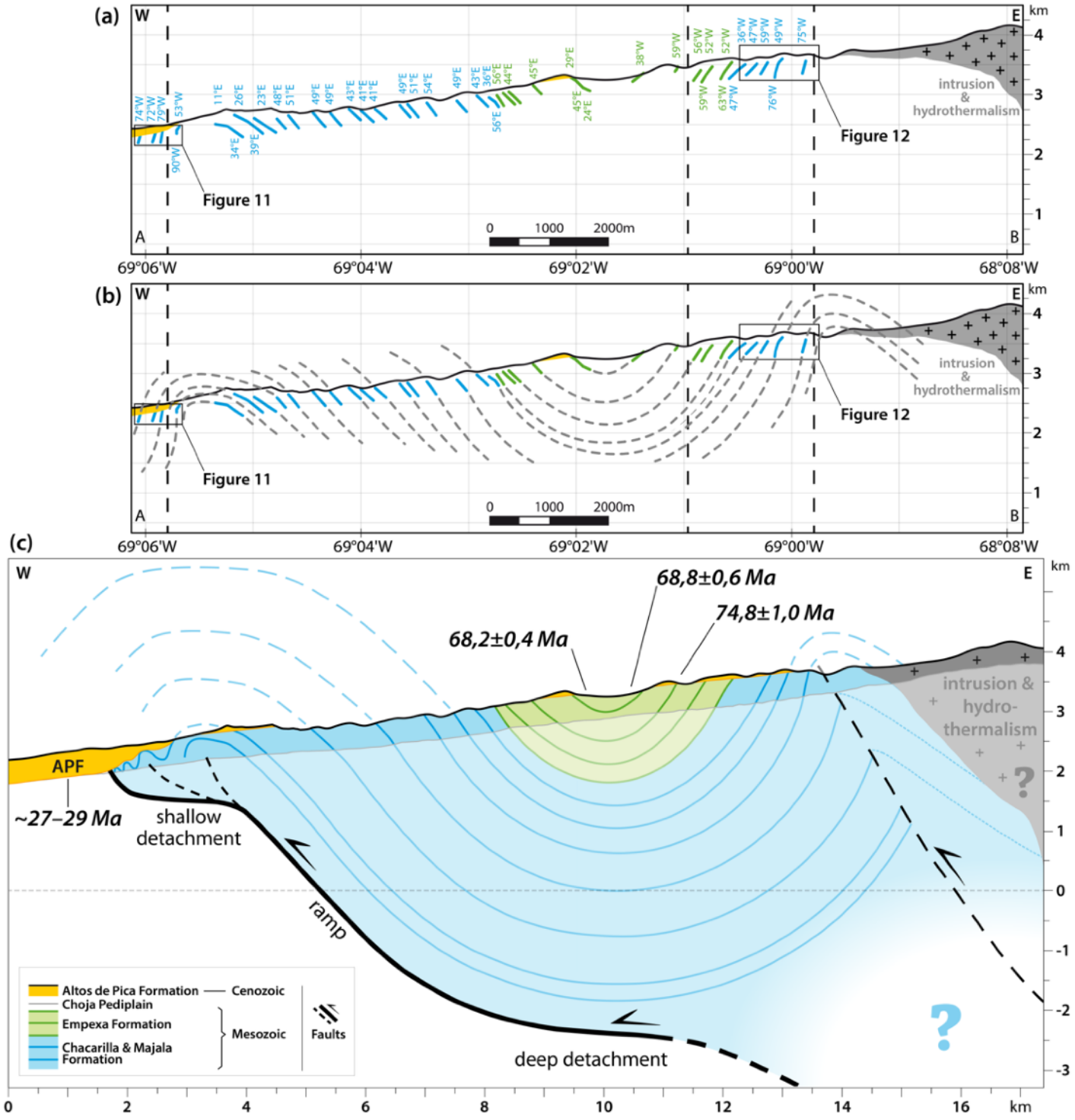

Figure 10. East–west cross-section of the Quebrada Blanca area, established from the projection of selected, well-expressed layers mapped on satellite imagery. APF: Altos de Pica Formation.

(a) Observations, reporting the geometry of projected layers and associated dip angles, together with their stratigraphic ages (color-code).

(b) Sub-surface interpretation and extrapolation of observations.

(c) Synthetic east–west cross-section based on (a) and (b). Interpretation at depth is indicated with transparent colors, in contrast with sub-surface observations. Extrapolation above the topographic surface is drawn with dashed lines. Ages from uranium-lead (U/Pb) radioisotope dating on zircon are taken from the Guatacondo geological map (Blanco and Tomlinson, 2012). The ~27–29 Ma age of the basal deposits of the Altos de Pica formation is derived from regional considerations (Victor et al., 2004).

514 geometry of layers from Jurassic to Cretaceous, we consider it minor for our analysis of the
515 folding here.

516 In the field, we observe small-scale deformation within both anticlines (Figure 10). A
517 series of anticlines with westward decreasing amplitude and wavelength (of a few tens to a few
518 hundreds of meters – to be compared to the ~4 km wavelength of the main anticline) are
519 observable on the western edge of the western anticline (Figures 10c and 11). In the field, at least
520 one of these small-scale folds seems affected by a minor thrust. Additionally, within the eastern
521 large-scale anticline, a thrust-affected small-scale fold is observed (Figures 10c and 12), and
522 confirms the west-vergence at this smaller scale.

523 The Cenozoic detrital units are unconformably deposited above the folded Mesozoic
524 series. Thin sheet-like river-incised Cenozoic surfaces remain in the central part, becoming more
525 dominant to the South and West (Figure 9). These superficial erosional surfaces show an overall
526 westward tilt (Figure 11). Westward thickening of the Cenozoic layers deposited above the
527 erosional Choja surface is clearly observed at the front of the western anticline (Figure 11) and
528 reveals the presence of growth strata.

529 5.3 Structural interpretations

530 As for the Pinchal area and by analogy with other FTBs, we interpret the Quebrada
531 Blanca area folds as related to ramp thrusts rooting onto a deep detachment (Figure 10c). The
532 detachment probably roots at least at the base of the observed Late Jurassic series, or possibly
533 deeper. Assuming constant layer thicknesses over the study area, it can be extrapolated that the
534 detachment locates at least 4 km beneath the current topographic surface (i.e. at least at –2 km
535 a.s.l.). To the East of our investigated area and in order to balance the proposed cross-section, the
536 detachment is interpreted to deepen. An alternative interpretation would be that the detachment
537 keeps a shallow eastward dip angle with some local thickening beneath the eastern anticline. The
538 secondary frontal folds with westward decreasing wavelength (Figures 10c and 11) can be
539 explained as disharmonic folds within the forelimb of the large western anticline and/or be
540 interpreted as reflecting the existence of a shallow thrust (Figure 10c). Such a feature is also in
541 good agreement with secondary (steeper) thrusts affecting the center of anticlines (Figure 10).

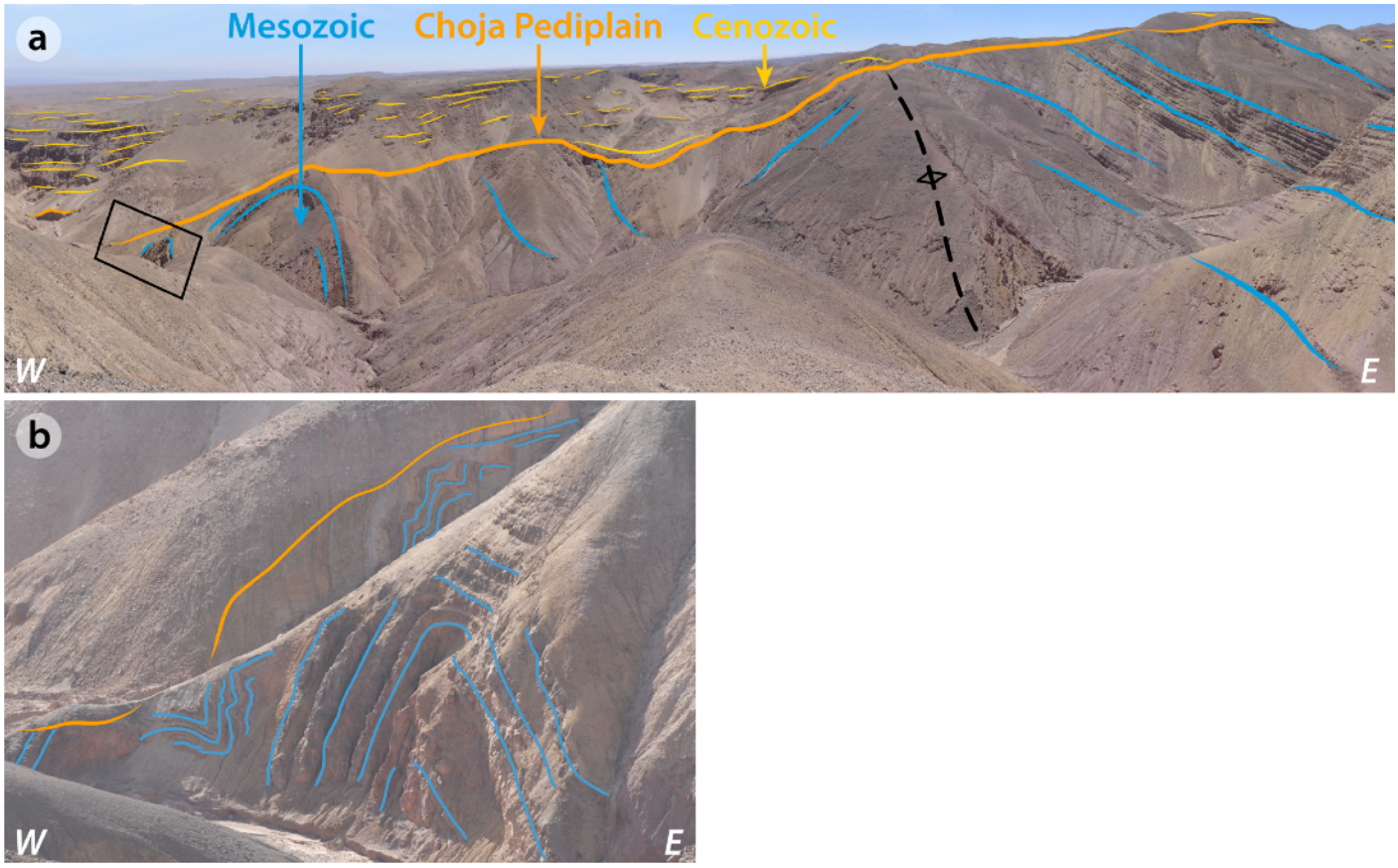

Figure 11. Field picture of the western limb of the western anticline in the Quebrada Blanca area. Non-interpreted photographs are provided in supporting material (Figure S18). Location on Figures 9 and 10.
(a) Series of folds with westward decreasing amplitude and wavelength (hundreds to tens of meters) observed at the front of the western anticline.
(b) Detailed view of the westernmost outcropping small-scale anticlines, located on (a) by the black box.

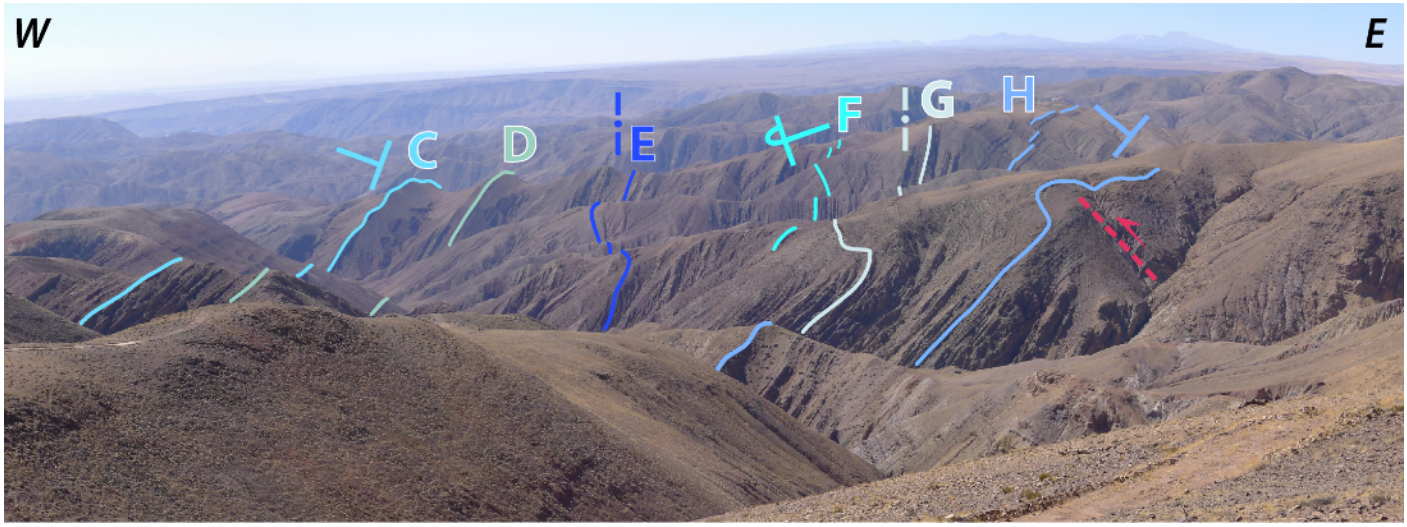

Figure 12. Landscape view on the western limb of the eastern large-scale anticline in the Quebrada Blanca area (Location on Figures 9 and 10). Here, steeply inclined Mesozoic horizons are very well discernible in the landscape. Bedding traces C, D, E, F, G and H underlined here are also georeferenced on the structural map (Figure 9) from mapping on satellite imagery. Note the thrust-affected small-scale fold (red dashed line) emphasizing the west-vergence of tectonic structures. The non-interpreted picture is provided in supporting material (Figure S19).

Line-length-balancing of the cross-section of Figure 10c results in ~3.8 km of shortening solely related to folding. This value is only a minimum as it does not account neither for slip on the interpreted thrusts nor for the observed small-scale deformation.

6. Kinematics of shortening of the fold-and-thrust-belt at the Pinchal and Quebrada Blanca sites

6.1 Timing of deformation

The time frame for the tectonic deformation observed within the two investigated sites can be bounded from our data, and more specifically from our results at the Quebrada Blanca site (Figure 10c). Indeed, our field observations and 3D-mapping do not reveal any relevant angular unconformity within the folded Mesozoic series in both study areas. The deformation of the investigated FTB therefore post-dates the deposition of these series. In the Quebrada Blanca area, the youngest folded Mesozoic layers that form the core of the mapped syncline belong to the Cerro Empexa Formation and bear U-Pb ages of 68.9±0.6 Ma and 68±0.4 Ma (Blanco & Tomlinson, 2013) (Figures 9 and 10c) . Here, we can therefore conclude that the deformation of the documented folds post-dates ~68 Ma.

Magmatic intrusions dated at ~44 Ma intruded the folded Mesozoic units, and appear cartographically not affected by folding (Blanco & Tomlinson, 2013) (Figure 9). This possibly suggests that the major part of the folding occurred during the ~68–44 Ma time interval. However, without additional observations of the deformation – or not – of these intrusions (geometry of the contact with surrounding host units, mineral deformation…), we cannot unequivocally conclude here from this simple cartographic observation.

Even though we suspect that the deformed series of the Pinchal zone are Triassic to Jurassic (section 4.2), we do not have any absolute ages of the folded units. Therefore, we postulate that deformation here also post-dates ~68 Ma by analogy to our observations at the Quebrada Blanca.

The FTB is unconformably covered by the Cenozoic deposits of the Altos de Pica Formation at both investigated sites. This is also the case for the ABT and secondary thrusts at few places in the Pinchal zone (Figure 4). The presence of growth strata at the front of the westernmost anticlines in both study areas, over the erosional Choja Pediplain, suggests that

571 some deformation proceeded after ~29 Ma, during deposition of the Altos de Pica Formation.
572 However, the deformation recorded by folded Mesozoic layers appears of greater intensity than
573 that of the Cenozoic growth layers (Figures 5c and 10c). Given this, we propose that the timing
574 of the main tectonic deformation at ~20–22ºS can be loosely bracketed to a maximum time span
575 of ~40 Myr, sometime between ~68 Ma and ~29 Ma, with additional relatively minor
576 deformation after ~29 Ma. Possibly, the main deformation period could be shorter (~24 Myr),
577 sometime between ~68 Ma and ~44 Ma, with minor shortening after the Eocene intrusions.

578 6.2 Further constraints on total shortening deduced from trishear modeling

579 Line-length-balancing only reveals a fraction of the shortening related to the folding of
580 the Mesozoic series. Because the deduced underlying faults of the FTBs have not reached the
581 surface (Figures 5c and 10c), we assume fault-propagation-folding to be the dominant mode of
582 deformation in the studied FTBs. To further explore and quantify the associated deformation, we
583 use kinematic trishear modeling (e.g., Allmendinger, 1998; Erslev, 1991) of the westernmost
584 anticlines documented at the Quebrada Tambillo (Pinchal area) and Quebrada Blanca. This
585 approach accounts for slip on propagating thrust-faults and models the deformation distributed at
586 the tip of these evolving faults. The trishear formalism relies on a set of parameters that are
587 adjusted here by trial and error so as to fit the deduced structural geometries of the modeled
588 anticlines. The values of these parameters are within the range considered in previous studies
589 (e.g., Allmendinger, 1998; Allmendinger & Shaw, 2000; Cristallini & Allmendinger, 2002;
590 Hardy & Ford, 1997; Zehnder & Allmendinger, 2000). Here we present our best-fitting model,
591 which allows for reproducing satisfactorily our structural results, acknowledging that it is most
592 probably not unique. From there, we further discuss the kinematics of the investigated sites.
593 Further details are provided in supplementary material. Tables S1 to S3 provide the set of
594 parameters used for our modeling.

595 The structural geometries of the westernmost anticlines of the two investigated sites are
596 reproduced, and the evolution of deformation is modeled over time taking into account the
597 Cenozoic growth strata. The final geometries of our best-fitting models are reported over our
598 cross-sections, represented in Figure 13. The various stages of deformation are shown in Figures
599 S20 and S21 in the supplementary material. We find that the geometries of the western anticlines
600 can be reproduced with a cumulative shortening of 3.1 km for Quebrada Tambillo (Pinchal area),

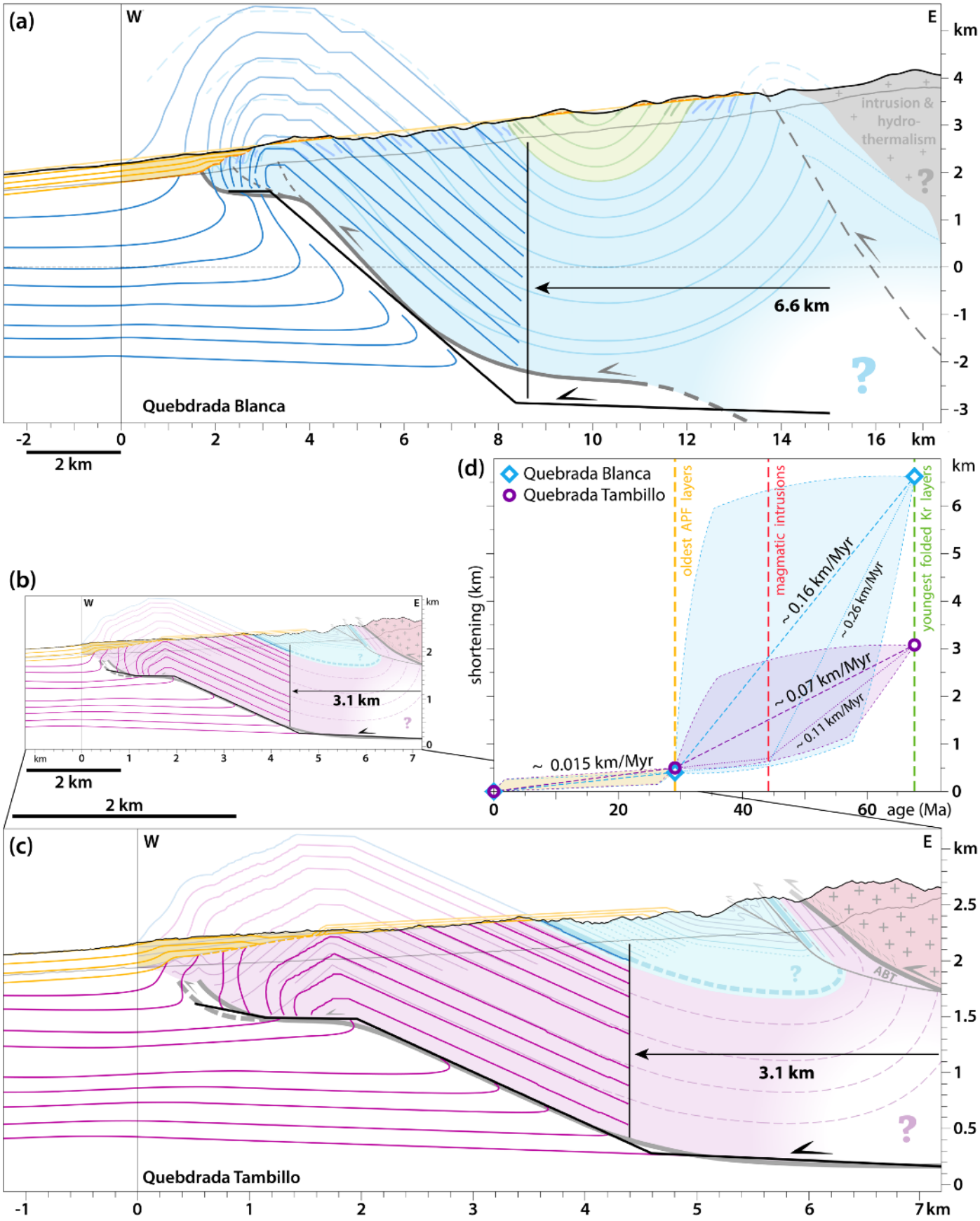

Figure 13. Caption on next page.

Figure 13. Kinematics of folding of the western anticlines of the Quebrada Blanca and Pinchal areas as deduced from field observations and trishear modeling. Modeling was performed with FaultFold Forward v.6 (Allmendinger, 1998).
(a-c) Final stages of the best-fit models in the case of **(a)** Quebrada Blanca area; **(b)** Quebrada Tambillo (Pinchal area), shown here at the same scale as (a). **(c)** Detailed and enlarged view of our results for Quebrada Tambillo (Pinchal area). Note the large scale-difference between the sections of the two investigated sites (a-b). Thicker lines outline model results, while transparent lines and colors refer to the cross-sections of Figures 10c and 5c. These lines are color-coded according to the stratigraphic level they represent, as in the original cross-sections. Black lines report the modeled thrusts and horizontal arrows report the model total shortening.
(d) Shortening vs. time, as deduced from trishear modeling of the western anticlines of the Quebrada Blanca and Pinchal areas, and the ages of deformed layers. The three temporal benchmarks correspond to the age of the youngest folded Cretaceous (Kr) unit (~68 Ma), to the age of magmatic intrusions (~44 Ma) that are cartographically discordant, both derived from the Guatacondo geological map (Blanco and Tomlinson, 2012 – see also Figures 9 and 10c), and to the ~29 Ma age of the oldest Cenozoic layer of the Altos de Pica Formation (APF) (Victor et al., 2004) above the Choja erosional surface. It is possible that most deformation occurred prior to ~44 Ma, as deduced from the age of the intrusions cartographically seemingly post-dating folding (Figure 9), even though this argument is to be taken with caution. Our results underline two phases of deformation, with a slowing down of deformation since ~29 Ma at least, possibly even before. Intermediate stages of the trishear modeling are reported on Figures S20 and S21 (supplementary material) for the cross-sections of Quebrada Tambillo and Quebrada Blanca, respectively. Model parameters are indicated in Tables S1–S3 in supplementary material.

and of 6.6 km for Quebrada Blanca (Figure 13). These values account for both thrusting and folding across the western anticlines. They are however minimum shortening values as (1) the depth of the detachment considered for modeling is minimal and could be deeper than the base of the outcropping units, and (2) the model formalism does not account for small-scale deformation, especially within the forelimb of the anticlines where the ramps approach the surface.

The above shortening values deduced from trishear modeling only account for the deformation (folding and thrusting) absorbed across the westernmost anticlines of our two investigated sites. If synclinal folding accounts for half of the shortening deduced previously by line-length-balancing in the Pinchal area (i.e. ~0.5 km of shortening), a minimum amount of shortening of ~3.6 km can be proposed across the whole Quebrada Tambillo section, and includes folding of the outcropping FTB, as well as slip on the detachment and western thrust ramp. When adding the minimum ~2.6 km of thrusting deduced on the ABT, we get a minimum shortening of ~6.2 km across the whole Pinchal area. Similarly, in the Quebrada Blanca area, if the easternmost anticline and syncline take up half of the folding deduced previously by line-length-balancing (i.e. ~2 km of shortening), a minimum amount of shortening of ~8.6 km is deduced across the whole Quebrada Blanca section, including folding of the outcropping FTB in addition to slip on the underlying detachment and western ramp.

The two investigated FTBs take up differing amounts of minimum shortening. These variations may relate to the disparate extents of outcropping structures, in particular because the scale of the two sections are significantly different, in terms of length (~7 km long section for the Quebrada Tambillo vs. ~17 km long section for the Quebrada Blanca) but also in terms of depth of the underlying detachment (altitude of ~0.2 km for Quebrada Tambillo vs. depth ~2 km for Quebrada Blanca, relative to sea level) (Figure 13). Lateral variations in deformation can also not be excluded.

6.3 Kinematics of shortening

Trishear modeling allows for simulating the evolution of thrust slip and folding in the case of the westernmost anticlines of the two investigated sites. By adding syntectonic layers while deformation proceeds, we also reproduce the overall geometry of the base of the Cenozoic Altos de Pica Formation deposits and of the subsequent growth strata (Figures S20 and S21). Syntectonic surfaces and layers are prescribed an initial 3–6° W dipping angle, similar to the

present-day overall regional topographic slope (Figure 1). From there, we find that ~0.5 km and ~0.4 km of shortening are needed to reproduce to the first order the geometry of the base of the Altos de Pica Formation deposits at the front of the Quebrada Tambillo (Pinchal area) and Quebrada Blanca sections, respectively, using the trishear models adjusted to the final cross-sections. When compared to the 3.1 km and 6.6 km of total shortening cumulated since ~68 Ma across the westernmost anticlines of these two sections, this indicates that the ~29 Ma old basal Cenozoic layers above the Choja surface only record at most 16% and 6% of this total shortening, respectively. We have tested the possibility of initial horizontal Cenozoic syntectonic layers. In this case, a post ~29 Ma shortening of 0.8 km at most is needed to best adjust the observed geometry of the basal Altos de Pica Formation layers, even though a good fit to both the geometry of the growth strata and of the finite fold structure cannot be satisfactorily found.

These results are then used to quantitatively describe the evolution of shortening over time across the westernmost anticlines of the two investigated sections, with account on the timing of deformation discussed in section 6.1 (Figure 13d). We find that shortening rates were on average of ~0.07–0.16 km/Myr over the time span ~68–29 Ma. They could have been even as high as ~0.11–0.26 km/Myr if considering that the main deformation phase is confined to ~68–44 Ma. Subsequently, deformation rates decreased to an average value of ~0.015 km/Myr after ~29 Ma, starting possibly earlier.

It should be noted that these average values are most probably minimum values. Indeed, thrusting and folding are here only modeled for the westernmost anticlines of our study sites, and do not account for the shortening cumulated neither across the other structures of the FTB nor on the ABT. Also, the main phase of deformation prior to ~29 Ma could have lasted less than the ~68–29 Ma or ~68–44 Ma time intervals, respectively (Figure 13d).

Our results therefore quantitatively emphasize our former qualitative conclusion that the major phase of deformation recorded at the two investigated sites occurred sometime between ~68 and ~29 Ma, with a significant subsequent slowing down of deformation rates afterwards, possibly as soon as ~44 Ma or earlier (Figure 13d).

7. Discussion

7.1 The Andean Basement Thrust

We have further documented the existence of a major west-vergent basement thrust – the ABT, for Andean Basement Thrust – along the western flank of the Andes, after its initial pointing out on earlier geological maps.

Our study in the Pinchal area suggests that the ABT bears local complexities with several strands and minor splays, most probably related to the reactivation of structures in the initial pre-Andean back-arc basins. Laterally and at a larger scale, these complexities may also exist so that the ABT is possibly segmented all along the west Andean flank at ~20–22ºS. The geological map of Skarmenta and Marinovic (1981), on which we based our investigations of the ABT, clearly documents this structure from ~21º15'S to 21º35'S, and possibly down to ~22°S with some structural complexities by ~21º35'S with the junction of two possible strands of this same basement thrust system.

Immediately north, the ABT is mapped locally as the Quehuita Fault up to ~21º11'S (Aguilef et al., 2019). The Choja Fault between ~21º08'S–21º01'S (Aguilef et al., 2019) is also mapped as a thrust bringing basement over folded Mesozoic sediments. Even though the cartographic continuity between both basement thrusts of Aguilef et al. (2019)'s map is not straightforward, they can be reasonably considered as strands of the same major basement thrust system, similar to that documented for the ABT in this study. North of ~21ºS, intrusions, hydrothermalism and surface volcanics hamper any clear observation of a similar basement thrust. Such basement thrust, if existent, would however provide a reasonable mechanism for the exhumation and exposure of basement rocks east of the folded Mesozoic units and at higher elevations, at the latitude of Quebrada Blanca (~20°45'S) (Figure 1). For these reasons, we cannot tell with any certainty whether a thrust contact similar to the ABT (bringing basement westward over folded Mesozoic) exists at this latitude, but such structure is to be suspected.

South of the map by Skarmenta and Marinovic (1981), in the Sierra Moreno at ~21°45'S, Haschke and Günther (2003)'s section report a basement thrust over folded Mesozoic units, in agreement with the style of deformation documented here, but with a relatively minor displacement on this thrust compared to our results in the Pinchal area. Together with the (1:1,000,000) Geological map of Chile (SERNAGEOMIN, 2003), Haschke and Günther

(2003)'s map suggests that the ABT is cartographically continuous southward to the southern end of the Sierra Moreno, at ~22°05'S. This possibly documents the lateral termination of this section of the ABT.

As a conclusion, the ABT stands as a major crustal structure, bringing basement units westward over folded Mesozoic units – and therefore uplifting the western margin of the Altiplano – possibly segmented but extending over at least ~120 km (Figure 1). Even though its various strands are mapped as local basement faults in some maps, as in our study (Figure 4) or in other maps (Aguilef et al., 2019; McElderry et al., 1996; Skarmenta & Marinovic, 1981; Tomlinson et al., 2001), altogether these thrust segments document a much larger thrust system (Figure 1). We interpret the ABT and the other thrusts west of it to root onto a low-angle, eastward dipping décollement, situated >2 km (Pinchal area) or >4 km (Quebrada Blanca area) beneath the present-day topographic surface. Deeper and eastward, this décollement probably steepens and forms a crustal-scale ramp, needed to sustain the uplift and topographic rise of the Western Andes, as proposed by Victor et al. (2004) and Armijo et al. (2015). Such crustal-scale structure is termed the West Andean Thrust (or WAT) by Armijo et al. (2015).

From the likely minimum offset of the basement in the Pinchal area we estimated that the ABT alone accommodated a strict minimum of ~2.6 km of shortening on a horizontal distance of ~1 km. This multi-kilometric shortening would be associated with multi-kilometric basement exhumation, but only limited thermochronological data actually permit to evaluate the amount of exhumation. These data presently exist at a regional scale but are absent locally. From apatite fission track dating in basement samples taken ~20 km east and south-east of our study sites of the Pinchal and Quebrada Blanca areas, Maksaev and Zentilli (1999) inferred at least 4–5 km of basement exhumation occurring between ~50–30 Ma. This is in good agreement with our results in terms of amount of uplift that would result from basement overthrusting on the ABT and above the WAT. In the absence of dated samples closer to the ABT, it is difficult to assess more precisely its timing. At a few places in the Pinchal area, the ABT is covered by Cenozoic deposits, so that it was probably mostly active before ~29 Ma. Given this observation and by comparison and extrapolation with published thermocronological results (Maksaev & Zentilli, 1999), we postulate that the ABT was most probably active between ~50–30 Ma, suggesting that it was therefore overall coeval with deformation of the FTB documented immediately further west.

719 ### 7.2 The West Andean Fold-and-Thrust-Belt at ~20–22ºS

720 The series of west-vergent folds and faults at ~20–22ºS deforming Mesozoic units is
721 interpreted as a west-vergent FTB, along the western flank of the Andes. By analogy to what has
722 been proposed at the latitude of Santiago de Chile (~33.5°S) (Armijo et al., 2015; Rauld, 2011;
723 Riesner et al., 2018, 2017), we propose to name this FTB hereafter as the West Andean Fold-
724 and-Thrust-Belt (WAFTB).

725 The WAFTB extends over our entire study zone from ~20–22ºS, even though a large part
726 north of the Quebrada Blanca area is covered by Cenozoic strata. It therefore spreads out over a
727 north–south-distance of at least ~200 km – and possibly more as folded Mesozoic sediments are
728 mapped on the (1:1,000,000) Geological map of Chile (SERNAGEOMIN, 2003) in the north-
729 and south-ward continuation of the zone investigated here. The WAFTB of northern Chile
730 accommodates a minimum shortening of ~3–9 km, as quantified from the ~7–17 km large cross-
731 sections representative of the two investigated areas (not including the contribution of the ABT
732 in the case of the Pinchal area).

733 Few authors attempted to quantify the shortening in this part of the Andes. At 20°30'S,
734 Victor et al. (2004) only evaluated the deformation affecting the post ~29 Ma deposits and not
735 the total shortening as could be derived from folded Mesozoic series. We further discuss their
736 results hereafter (below and section 7.3). At ~21°45'S, ~30 km south of the Pinchal area,
737 Haschke and Günther (2003) reported a minimum shortening of >9 km from a ~50 km wide
738 cross-section, but without providing nor discussing the data used to make this estimate. Their
739 section encompasses an equivalent of the WAFTB and ABT investigated in this study in the
740 Sierra Moreno area, but also extends further east. Within the ~8–10 km wide Sierra Moreno area
741 itself, they estimate a minimum shortening of ~4 km, a value consistent with our results. This
742 study of Haschke and Günther (2003) is to our knowledge the only other work attempting to
743 estimate the minimum total shortening absorbed by the WAFTB at 20–22°S. It becomes obvious
744 that the various structures of the WAFTB in northern Chile, wherever they are (Quebrada
745 Blanca, Pinchal or Sierra Moreno areas), all absorb multi-kilometric shortening, at the scale of
746 only one to three major folds and thrusts.

747 To the West and laterally, the WAFTB is covered by Cenozoic deposits. Seismic profiles
748 from the chilean Empresa Nacional del Petroleo (ENAP), as re-interpreted by Victor et al.
749 (2004), Jordan et al. (2010) or Labbé et al. (2019), show a series of several blind west-verging

thrust-faults affecting both the Cenozoic and the underlying Mesozoic units. Nonetheless, deformation is mostly well-imaged for post ~29 Ma growth strata within the Cenozoic series deposited above the Choja erosional surface, and remains less well-resolved for underlying Mesozoic units. These observations may reflect the fact that Mesozoic units are much more deformed than Cenozoic layers, a deduction in line with our own field observations in the Pinchal and Quebrada Blanca areas (Figures 4 and 9). As proposed by Victor et al. (2004) and Armijo et al. (2015), the west-vergent thrust-faults beneath the western Andean flank at ~20–22°S, can reasonably be interpreted as connecting onto an east-dipping detachment, deepening towards the mountain range, again in line with our interpretation of the structure in our study areas (Figures 5c and 10c). Altogether, these data suggest that all these thrust faults, either blind or deduced from outcropping folds, pertain to the same WAFTB system. The WAFTB at ~20–22°S therefore extends over a much wider region (~50 km, maybe locally more) than the two ~7–17 km wide sites investigated in this study (Figure 1), as most of the FTB is hidden beneath the less deformed Cenozoic cover (Figure 1). This conclusion further emphasizes that the minimum ~3–9 km of shortening proposed here from the folds of the Quebrada Blanca and Pinchal areas (when excluding the contribution of the ABT in the Pinchal area) are clearly under-estimates of the total shortening across the whole WAFTB at this latitude. A precise quantification of the deformation recorded by buried folded Mesozoic units west of our study sites is not possible from available seismic profiles (Victor et al., 2004; Jordan et al., 2010; Labbé et al., 2019). The amount of ~20–30 km of total shortening along the western flank of the Andes qualitatively estimated by Armijo et al. (2015) would be a reasonable value at scale with the structural relief of the western flank and the crustal thickness beneath.

7.3 Temporal evolution of deformation

Our investigations underline that the deformation of the Quebrada Blanca and Pinchal areas is not linearly distributed over time, and can be assigned to two main periods: (1) a period of major deformation sometime between ~68–29 Ma (possibly ~68–44 Ma) at a minimum average shortening rate of ~0.1–0.3 km/Myr; and (2) a subsequent period of moderate deformation from ~29–0 Ma (starting possibly earlier) at an average rate of <0.1 km/Myr (Figure 13d). These deductions and rates hold for the westernmost anticline of the study sites, but the reduction in deformation rates is expected at the scale of both whole investigated sites. Indeed,

780 the difference in the deformation cumulated by Mesozoic units and by post ~29 Ma Cenozoic
781 layers can be qualitatively – but clearly – intuited from our cross-sections (Figures 5, 10 and 13).
782 Westward, it may also be inferred but with less certainty from the ENAP seismic profiles (see
783 discussion above). This deformation slow-down, starting by ~29 Ma and possibly earlier, could
784 therefore be regional across the entire WAFTB.

785 The period of major deformation deduced at the scale of the WAFTB sections
786 investigated here, sometime from ~68 Ma to ~29 Ma (even possibly to ~44 Ma), is coeval to the
787 first order with the timing of basement exhumation deduced from thermochronology by Maksaev
788 and Zentilli (1999), and with the timing postulated for thrusting on the ABT (see section 7.1).
789 The proposed time window is also consistent with the main Incaic phase of deformation inferred
790 by various authors as the main period of Andean mountain-building stricto sensu (e.g., Charrier
791 et al., 2007; Cornejo et al., 2003; Pardo–Casas & Molnar, 1987; Steinmann, 1929).

792 Based on the ENAP seismic profiles in the westward prolongation of our study areas,
793 Victor et al. (2004) investigated the folding and thrusting recorded by the growth strata of the
794 Cenozoic Altos de Pica Formation. They determined a post ~29 Ma shortening of ~3 km,
795 accommodated by several west-vergent thrusts within the ~40 km wide Atacama Bench. In both
796 our study areas, we were able to reproduce with trishear modeling the first-order pattern of the
797 slightly deformed Cenozoic growth strata over and in front of the western anticlines. We found
798 ~0.4–0.5 km of post ~29 Ma shortening on one single most frontal fault and fold for our two (~7
799 and ~17 km long) investigated sections (Figures S20, S21). These values are in overall good
800 agreement with the results of Victor et al. (2004) when setting them to the same spatial scale.
801 Compared to the minimum ~3–6 km of ante ~29 Ma shortening quantified on one single
802 structure from each study section (Figures S20, S21), the post ~29 Ma shortening is clearly of
803 limited importance.

804 The simplest interpretation would be that this post ~29 Ma decline of the shortening rate
805 results from the slow-down of the same protracted compressional event which caused the
806 formation of the west-vergent WAFTB and ABT. With the presently available data at 20–22°S,
807 we cannot exclude that this slow-down may have started even before ~29 Ma – possibly as soon
808 as ~44 Ma, or even before (section 6.3) – but definitely not afterwards. Anyhow, in the absence
809 of sedimentary markers that would provide further quantitative details on the incremental
810 deformation between ~68 Ma and ~29 Ma, the evolution of shortening cannot be quantified more

precisely over time, and only average rates can be proposed over the large time spans of the phases of major and moderate deformation.

8 Conclusion: Contribution of the western Andes to mountain-building at ~20–22°S

In this study, we investigate and explore two major structural features within the western flank of the Andes at ~20–22°S: (1) the Andean Basement Thrust (ABT), which stands as a west-vergent, >120 km long system of ~north–south trending thrusts bringing Paleozoic basement over folded Mesozoic series; (2) the West Andean Fold-and-Thrust-Belt (WAFTB), which is a west-vergent FTB deforming Mesozoic and Cenozoic sediments, mostly covered by the Cenozoic Altos de Pica Formation, but cropping out in few (up to ~10–20 km wide) places along the mountain flank. The WAFTB extends over at least ~200 km north–south. Even though our investigations only rely on two limited outcropping sites, our deductions have regional implications when compared and set on scale with previous results.

Using field and satellite observations, we build structural cross-sections and quantify the recorded shortening at two key sites along the western mountain flank. We find a minimum shortening of ≥2.6 km on the ABT and of ≥3–9 km on the few exposed structures of the WAFTB. This strict minimum shortening – derived from outcrop areas of limited extent – corresponds only to a fraction of the entire deformation at the scale of the whole Western Cordillera at ~20–22ºS. When set on scale with the extent of the investigated structures, it clearly implies the possibility of multi-kilometric shortening across the western flank of the Andes.

We further exploit the differential deformation recorded by folded Mesozoic layers and Cenozoic growth strata of the post ~29 Ma Altos de Pica Formation. We show that the outcropping WAFTB was mainly active between ~68–29 Ma (possibly ~68–44 Ma), and that its deformation rates significantly decreased after ~29 Ma (or starting sometime before). By comparison to previous studies of the blind portions of the WAFTB west of our study sites, we propose that such slow-down of deformation rates was regional rather than local. In addition, field observations and published thermochronological results of basement exhumation suggest that this temporal evolution of deformation rates also holds for the ABT. We therefore propose that the post ~29 Ma decline in shortening rates resulted from the regional slow-down of the same protracted compressional event that caused the formation of the west-vergent WAFTB and ABT.

Even though multi-kilometric, the shortening accommodated by the west-vergent structures of the western Andes outlined in this study represents a minor contribution to the total crustal shortening of >300 km across the entire Central Andes at ~20ºS (e.g., Anderson et al., 2017; Barnes & Ehlers, 2009; Elger et al., 2005; Kley & Monaldi, 1998; McQuarrie et al., 2005; Oncken et al., 2012; Sheffels, 1990). It should however be recalled that this deformation took place mostly in the early stages of the Andean orogeny, sometime between ~68–29 Ma (possibly ~68–44 Ma), during the so-called Incaic phase. In fact, when replaced within the temporal evolution of Andean mountain-building at these latitudes (e.g., Armijo et al., 2015; Charrier et al., 2007; McQuarrie et al., 2005; Oncken et al., 2006), the early multi-kilometric shortening evidenced here represents a major contribution to initial Andean deformation, which has been most often neglected. The slowing down of deformation across the western Andean flank by ~29 Ma – and possibly starting before – may have accompanied the jumping and transfer of deformation towards the East on east-vergent structures (i.e. towards the eastern Altiplano and further east, e.g., Isacks et al., 1988; McQuarrie et al., 2005; Oncken et al., 2006), building from there a bi-vergent orogen (e.g., Armijo et al., 2015; Faccenna et al., 2013; Martinod et al., 2020). As such, the early stages of Andean deformation described here at ~20–22°S recall the first-order kinematics of crustal shortening deduced for the ~20–25 Myr old growing Andes at ~33.5°S (Riesner et al., 2018, 2019). This analogy suggests the continuity of the WAT all along the western flank of the Central Andes, re-sketching the relevance of this structure in the earlier stages of the Andean orogeny.

Acknowledgements

This study was supported by grants from CNRS-INSU (program TELLUS-SYSTER) and from the Institut de physique du globe de Paris (IPGP). Field work was also funded by the Andean Tectonics Laboratory of the Advanced Mining Technology Center, University of Chile. Earlier work on this zone by RL and DC was supported by ANR project MegaChile (grant ANR-12-BS06-0004-02) and LABEX UnivEarthS project. TH benefitted from a PhD grant attributed by the French Ministry of Higher Education and Research. Pleiades satellite imagery was obtained through the ISIS program of the CNES under an academic license and is not for open distribution. The authors thank A. Delorme for his technical assistance in producing the DEMs.

Numerical computations for the DEMs were performed on the S-CAPAD platform, Institut de physique du globe de Paris (IPGP). The kinematic modeling was made using FoldFault Forward version 6, freely available from http://www.geo.cornell.edu/geology/faculty/RWA/programs/faultfoldforward.html (Allmendinger, 1998). R. Armijo and the late R. Thiele are warmly thanked for the fruitful discussions that led over the years to this work and manuscript. We also benefited from discussions with C. Creixell, N. Blanco, A. Tomlinson and F. Sepulveda (SERNAGEOMIN), from the valuable help of M. Riesner for the 3D mapping, and that of L. Barrier for facies and polarity identifications. L. Barrier and N. Bellhasen are also thanked for discussions that inspired and led to trishear modeling. This study was partly supported by IdEx Université de Paris ANR-18-IDEX-0001. This is IPGP contribution number XXX.

References

Aguilef, S., Franco, C., Tomlinson, A., Blanco, N., Alvarez, J., Montecino, D., et al. (2019). *Geología del área Quehuita-Chela, regiones de Tarapacá y Antofagasta*. Servicio Nacional de Geología y Minería (Carta Geológica de Chile, Serie Geología Básica 207: 293 p.,1 mapa escala 1:100,000). Santiago, Chile.

Allmendinger, R. W. (1998). Inverse and forward numerical modeling of trishear fault-propagation folds. *Tectonics, 17*(4), 640–656. https://doi.org/10.1029/98TC01907

Allmendinger, R. W., & Shaw, J. H. (2000). Estimation of fault propagation distance from fold shape: Implications for earthquake hazard assessment. *Geology, 28*(12), 1099–1102.

Anderson, R. B., Long, S. P., Horton, B. K., Calle, A. Z., & Ramirez, V. (2017). Shortening and structural architecture of the Andean fold-thrust belt of southern Bolivia (21°S): Implications for kinematic development and crustal thickening of the central Andes. *Geosphere, 13*(2), 538–558. https://doi.org/10.1130/GES01433.1

Armijo, R., Rauld, R., Thiele, R., Vargas, G., Campos, J., Lacassin, R., & Kausel, E. (2010). The West Andean Thrust, the San Ramón Fault, and the seismic hazard for Santiago, Chile. *Tectonics, 29*(TC2007). https://doi.org/10.1029/2008TC002427

Armijo, R., Lacassin, R., Coudurier-Curveur, A., & Carrizo, D. (2015). Coupled tectonic evolution of Andean orogeny and global climate. *Earth-Science Reviews, 143*, 1–35. https://doi.org/10.1016/j.earscirev.2015.01.005

Baker, M. C. W. (1977). Geochronology of upper Tertiary volcanic activity in the Andes of north Chile. *Geologische Rundschau, 66*(1), 455–465. https://doi.org/10.1007/BF01989588

Barnes, J., Ehlers, T., McQuarrie, N., O'Sullivan, P., & Tawackoli, S. (2008). Thermochronometer record of Central Andean Plateau growth, Bolivia (19.5°S). *Tectonics, 27*(TC3003). https://doi.org/10.1029/2007TC002174

Barnes, J. B., & Ehlers, T. A. (2009). End member models for Andean Plateau uplift. *Earth-Science Reviews, 97*(1–4), 105–132. https://doi.org/10.1016/j.earscirev.2009.08.003

Blanco, N., & Tomlinson, A. J. (2013). *Carta Guatacondo, Region de Tarapaca*. (Carta Geologica de Chile, Serie Geologia Basica). Santiago, Chile: Servicio Nacional de Geología y Minería.

Blanco, N., Tomlinson, A. J., Moreno, K., & Rubilar, D. (2000). *Importancia estratigráfica de icnitas de dinosaurios en la Fm. Chacarilla (Jurásico Superior - Cretácico Inferior), I Región, Chile*. Presented at the IX Congreso Geológico Chileno. Servicio Nacional de Geología y Minería, Puerto Varas, Chile.

Blanco, N., Vásquez, P., Sepúlveda, F., Tomlinson, A. J., Quezada, A., & Ladino, M. (2012). *Levantamiento Geológico para el Fomento de la Exploración de Recursos Minerales e Hídricos de la Cordillera de la Costa, Depresión Central y Precordillera de la Región de Tarapacá (20°–21°S)*. (Informe Registrado IR-12-50, 246 p., 7 maps, scale 1:100,000). Santiago, Chile: Servicio Nacional de Geología y Minería.

Brooks, B. A., Bevis, M., Whipple, K., Ramon Arrowsmith, J., Foster, J., Zapata, T., et al. (2011). Orogenic-wedge deformation and potential for great earthquakes in the central Andean backarc. *Nature Geoscience, 4*(6), 380–383. https://doi.org/10.1038/ngeo1143

Buchelt, M., & Tellez, C. (1988). The Jurassic La Negra Formation in the area of Antofagasta, northern Chile (lithology, petrography, geochemistry). In *The Southern Central Andes* (Springer-Verlag Berlin Heidelberg, Vol. 17, pp. 169–182). https://doi.org/10.1007/BFb0045181

Charrier, R., Pinto, L., & Rodríguez, M. P. (2007). Tectonostratigraphic evolution of the Andean Orogen in Chile. In T. Moreno & W. Gibbons (Eds.), *The Geology of Chile* (First, pp. 21–114). The Geological Society of London. https://doi.org/10.1144/GOCH.3

Cornejo, P., Matthews, S., & Pérez de Arce, C. (2003). The "K-T" compressive deformation event in northern Chile (24°–27°S). In E. Campos (Eds), *X Congreso Geológico Chileno Actas*, Concepción, Chile, (Thematic Session ST1, p. 1–13,CD-ROM).

Cristallini, E. O., & Allmendinger, R. W. (2002). Backlimb trishear: a kinematic model for curved folds developed over angular fault bends. *Journal of Structural Geology, 24*(2), 289–295. https://doi.org/10.1016/S0191-8141(01)00063-3

DeCelles, P. G., Zandt, G., Beck, S. L., Currie, C. A., Ducea, M. N., Kapp, P., et al. (2015). Cyclical orogenic processes in the Cenozoic central Andes. In P. G. DeCelles, M. N. Ducea, B. Carrapa, & P. A. Kapp, *Geodynamics of a Cordilleran Orogenic System: The Central Andes of Argentina and Northern Chile*. Geological Society of America. https://doi.org/10.1130/2015.1212(22)

DeMets, C., Gordon, R., Argus, D., & Stein, S. (1994). Effect of recent revisions to the geomagnetic reversal time scale on estimates of current plate motions. *Geophysical Research Letters*, 21. https://doi.org/10.1029/94GL02118

Dingman, R. J., & Galli, C. O. (1965). *Geology and Ground-Water Resources of the Pica Area, Tarapaca Province, Chile*. Geological Survey Bulletin 1189. US Dept of Interior.

Elger, K., Oncken, O., & Glodny, J. (2005). Plateau-style accumulation of deformation: Southern Altiplano. *Tectonics, 24*(4). https://doi.org/10.1029/2004TC001675

Erslev, E. A. (1991). Trishear fault-propagation folding. *Geology, 19*, 617–620. https://doi.org/10.1130/0091-7613(1991)019<0617:TFPF>2.3.CO;2

Faccenna, C., Becker, T. W., Conrad, C. P., & Husson, L. (2013). Mountain building and mantle dynamics. *Tectonics, 32*(1), 80–93. https://doi.org/10.1029/2012TC003176

Faccenna, C., Oncken, O., Holt, A. F., & Becker, T. W. (2017). Initiation of the Andean orogeny by lower mantle subduction. *Earth and Planetary Science Letters, 463*, 189–201. https://doi.org/10.1016/j.epsl.2017.01.041

954 Farías, M., Charrier, R., Comte, D., Martinod, J., & Hérail, G. (2005). Late Cenozoic
955 deformation and uplift of the western flank of the Altiplano: Evidence from the
956 depositional, tectonic, and geomorphologic evolution and shallow seismic activity
957 (northern Chile at 19°30′S): Western Altiplano Uplift. *Tectonics, 24*(4), TC4001.
958 https://doi.org/10.1029/2004TC001667

959 Galli, C., & Dingman, R. J. (1962). *Cuadrángulos Pica, Alca, Matilla y Chacarilla: Con un*
960 *estudio sobre los recursos de agua subterránea, Provincia de Tarapacá*. Instituto de
961 Investigaciones Geológicas (Carta Geológica de Chile 7–10, 125 p., 4 maps, scale
962 1:50,000).

963 Galli-Olivier, C. (1967). Pediplain in Northern Chile and the Andean Uplift. *Science, 158*(3801),
964 653–655. https://doi.org/10.1126/science.158.3801.653

965 Garcia, M., & Hérail, G. (2005). Fault-related folding, drainage network evolution and valley
966 incision during the Neogene in the Andean Precordillera of Northern Chile.
967 *Geomorphology, 65*(3–4), 279–300. https://doi.org/10.1016/j.geomorph.2004.09.007

968 Hardy, S., & Ford, M. (1997). Numerical modeling of trishear fault propagation folding.
969 *Tectonics, 16*(5), 841–854. https://doi.org/10.1029/97TC01171

970 Haschke, M., & Günther, A. (2003). Balancing crustal thickening in arcs by tectonic vs.
971 magmatic means. *Geology, 31*(11), 933. https://doi.org/10.1130/G19945.1

972 Heit, B., Sodoudi, F., Yuan, X., Bianchi, M., & Kind, R. (2007). An S receiver function analysis
973 of the lithospheric structure in South America. *Geophysical Research Letters, 34*(14).
974 https://doi.org/10.1029/2007GL030317

975 Homewood, P., & Lateltin, O. (1988). Classic Swiss Clastics (Flysch and Molasse) - The Alpine
976 connection. *Geodinamica Acta, 2*(1), 1–11.
977 https://doi.org/10.1080/09853111.1988.11105150

978 Isacks, B. L. (1988). Uplift of the Central Andean Plateau and bending of the Bolivian Orocline.
979 *Journal of Geophysical Research, 93*(B4), 3211–3231.
980 https://doi.org/10.1029/JB093iB04p03211

Kley, J., & Monaldi, C. R. (1998). Tectonic shortening and crustal thickness in the Central Andes: How good is the correlation? *Geology, 26*(8), 723–726. https://doi.org/10.1130/0091-7613(1998)026<0723:TSACTI>2.3.CO;2

Lamb, S. (2011). Did shortening in thick crust cause rapid Late Cenozoic uplift in the northern Bolivian Andes? *Journal of the Geological Society, 168*(5), 1079–1092. https://doi.org/10.1144/0016-76492011-008

Lamb, S. (2016). Cenozoic uplift of the Central Andes in northern Chile and Bolivia – reconciling paleoaltimetry with the geological evolution. *Canadian Journal of Earth Sciences, 53*(11), 1227–1245. https://doi.org/10.1139/cjes-2015-0071

Lucassen, F., Becchio, R., Wilke, H. G., Franz, G., Thirlwall, M. F., Viramonte, J., & Wemmer, K. (2000). Proterozoic–Paleozoic development of the basement of the Central Andes (18–26°S) – a mobile belt of the South American craton. *Journal of South American Earth Sciences, 13*(8), 697–715. https://doi.org/10.1016/S0895-9811(00)00057-2

Martinod, J., Gérault, M., Husson, L., & Regard, V. (2020). Widening of the Andes: An interplay between subduction dynamics and crustal wedge tectonics. *Earth-Science Reviews, 204*, 103170. https://doi.org/10.1016/j.earscirev.2020.103170

McElderry, S., Chong, G., Prior, D., & Flint, S. S. (1996). *Structural styles in the Domeyko range, northern Chile*. In Géodynamique andine : résumés étendus, Paris : ORSTOM, 439-442. Third International Symposium on Andean Geodynamics (ISAG), Saint-Malo, France, 1996/09/17-19. ISBN 2-7099-1332-1. Retrieved from https://horizon.documentation.ird.fr/exl-doc/pleins_textes/divers4/010008618.pdf

McQuarrie, N., Horton, B. K., Zandt, G., Beck, S., & DeCelles, P. G. (2005). Lithospheric evolution of the Andean fold–thrust belt, Bolivia, and the origin of the central Andean plateau. *Tectonophysics, 399*(1–4), 15–37. https://doi.org/10.1016/j.tecto.2004.12.013

Mpodozis, C., & Ramos, V. A. (1989). The Andes of Chile and Argentina. In G. E. Ericksen, M. T. Canas Pinochet, & J. A. Reinemund (Eds.), *Geology of the Andes and its Relation to Hydrocarbon and Mineral Resources* (pp. 59–90). Circum-Pacific Council for Energy and Mineral Resources Earth Sciences Series, Houston, Texas.

1009 Muñoz, N., & Charrier, R. (1996). Uplift of the western border of the Altiplano on a west-
1010 vergent thrust system, Northern Chile. *Journal of South American Earth Sciences, 9*(3–
1011 4), 171–181. https://doi.org/10.1016/0895-9811(96)00004-1

1012 Norabuena, E., Leffler-Griffin, L., Mao, A., Dixon, T., Stein, S., Sacks, I. S., et al. (1998). Space
1013 geodetic observations of Nazca–South America convergence across the Central Andes.
1014 *Science, 279*(5349), 358–362. https://doi.org/10.1126/science.279.5349.358

1015 Oncken, O., Boutelier, D., Dresen, G., & Schemmann, K. (2012). Strain accumulation controls
1016 failure of a plate boundary zone: Linking deformation of the Central Andes and
1017 lithosphere mechanics. *Geochemistry, Geophysics, Geosystems, 13*(Q12007).
1018 https://doi.org/10.1029/2012GC004280

1019 Oncken, Onno, Chong, G., Franz, G., Giese, P., Götze, H.-J., Ramos, V. A., et al. (Eds.). (2006).
1020 *The Andes: Active Subduction Orogeny*. Berlin, Heidelberg: Springer. Retrieved from
1021 https://doi.org/10.1007/978-3-540-48684-8

1022 Pardo-Casas, F., & Molnar, P. (1987). Relative motion of the Nazca (Farallon) and South
1023 American Plates since Late Cretaceous time. *Tectonics, 6*(3), 233–248.
1024 https://doi.org/10.1029/TC006i003p00233

1025 Ramos, V. A. (1988). Late Proterozoic - Early Paleozoic of South America – a Colisional
1026 History. *Episodes, 11*(3), 7.

1027 Ramos, V. A. (2008). The Basement of the Central Andes: The Arequipa and Related Terranes.
1028 *Annual Review of Earth and Planetary Sciences, 36*(1), 289–324.
1029 https://doi.org/10.1146/annurev.earth.36.031207.124304

1030 Rapela, C. W., Pankhurst, R. J., Casquet, C., Baldo, E., Saavedra, J., & Galindo, C. (1998). Early
1031 evolution of the Proto-Andean margin of South America. *Geology, 26*(8), 707–710.

1032 Rauld, R. A. (2011). *Deformación cortical y peligro sísmico asociado a la falla San Ramón en el*
1033 *frente cordillerano de Santiago, Chile Central (33ºS)*, (Doctoral dissertation). Retrieved
1034 from http://www.tesis.uchile.cl/tesis/uchile/2011/cf-rauld_rp/html/index.html. Dep. de
1035 Geol., Univ. de Chile, Santiago.

1036 Riesner, M., Lacassin, R., Simoes, M., Armijo, R., Rauld, R., & Vargas, G. (2017). Kinematics
1037 of the active West Andean fold-and-thrust belt (central Chile): Structure and long-term
1038 shortening rate. Tectonics, 36(2), 287–303. https://doi.org/10.1002/2016TC004269

1039 Riesner, Magali, Lacassin, R., Simoes, M., Carrizo, D., & Armijo, R. (2018). Revisiting the
1040 Crustal Structure and Kinematics of the Central Andes at 33.5°S: Implications for the
1041 Mechanics of Andean Mountain Building. *Tectonics, 37*(5), 1347–1375.
1042 https://doi.org/10.1002/2017TC004513

1043 Riesner, Magali, Simoes, M., Carrizo, D., & Lacassin, R. (2019). Early exhumation of the
1044 Frontal Cordillera (Southern Central Andes) and implications for Andean mountain-
1045 building at ~33.5°S. *Scientific Reports, 9*(7972). https://doi.org/10.1038/s41598-019-
1046 44320-1

1047 Rosu, A.-M., Deseilligny, M., Delorme, A., Binet, R., & Klinger, Y. (2014). Measurement of
1048 ground displacement from optical satellite image correlation using the free open-source
1049 software MicMac. *ISPRS Journal of Photogrammetry and Remote Sensing, 100*.
1050 https://doi.org/10.1016/j.isprsjprs.2014.03.002

1051 Rupnik, E., Deseilligny, M., Delorme, A., & Klinger, Y. (2016). Refined satellite image
1052 orientation in the free open-source photogrammetric tools Apero/Micmac. *ISPRS Annals*
1053 *of Photogrammetry, Remote Sensing and Spatial Information Sciences, III–1*, 83–90.
1054 https://doi.org/10.5194/isprs-annals-III-1-83-2016

1055 SERNAGEOMIN. (2003). Mapa Geológico de Chile: versión digital. (No. 4, CD-ROM, versión
1056 1.0, 2003). Santiago, Chile: Servicio Nacional de Geología y Minería, Publicación
1057 Geológica Digital.

1058 Sheffels, B. M. (1990). Lower bound on the amount of crustal shortening, in the central Bolivian
1059 Andes. *Geology, 18*(9), 812–815. https://doi.org/10.1130/0091-
1060 7613(1990)018<0812:LBOTAO>2.3.CO;2

1061 Skarmenta, J., & Marinovic, N. (1981). *Hoja Quillagua*. Inst. Invest. Geol. (Carta Geol. de Chile
1062 No.51, 1:250,000)

1063 Steinmann, G. (1929). Geologie von Peru. *The Journal of Geology, Vol 38*, No 2, University of
1064 Chicago. https://doi.org/10.1086/623704

1065 Tassara, A., Götze, H.-J., Schmidt, S., & Hackney, R. (2006). Three-dimensional density model
1066 of the Nazca plate and the Andean continental margin. *Journal of Geophysical Research:*
1067 *Solid Earth, 111*(B09404). https://doi.org/10.1029/2005JB003976

1068 Tomlinson, A., Blanco, N., Maksaev, V., Dilles, J., Grunder, A., & Ladino, M. (2001). *Geología*
1069 *de la Precordillera Andina de Quebrada Blanca-Chuquicamata, Regiones I y II (20°30'-*
1070 *22°30'S)*. Informe Registrado IR-01-20.

1071 Tomlinson, A. J., Blanco, N., & Ladino, M. (2015). *Carta Mamina, Región de Tarapacá*. (Carta
1072 Geológica de Chile, Serie Geología Básica, scale 1:100,000). Santiago, Chile: Servicio
1073 Nacional de Geología y Minería.

1074 Vergara, H., & Thomas, A. (1984). *Hoja Collacagua, Región de Tarapacá*. (scale 1:250.000).
1075 Santiago, Chile: Servicio Nacional de Geología y Minería.

1076 Victor, P., Oncken, O., & Glodny, J. (2004). Uplift of the western Altiplano plateau: Evidence
1077 from the Precordillera between 20° and 21°S (northern Chile): Altiplano West Flank.
1078 *Tectonics, 23*(4). https://doi.org/10.1029/2003TC001519

1079 Wölbern, I., Heit, B., Yuan, X., Asch, G., Kind, R., Viramonte, J., et al. (2009). Receiver
1080 function images from the Moho and the slab beneath the Altiplano and Puna plateaus in
1081 the Central Andes. *Geophysical Journal International, 177*(1), 296–308.
1082 https://doi.org/10.1111/j.1365-246X.2008.04075.x

1083 Yuan, X., Sobolev, S. V., Kind, R., Oncken, O., Bock, G., Asch, G., et al. (2000). Subduction
1084 and collision processes in the Central Andes constrained by converted seismic phases.
1085 *Nature, 408*(6815), 958–961. https://doi.org/10.1038/35050073

1086 Zandt, G., Velasco, A. A., & Beck, S. L. (1994). Composition and thickness of the southern
1087 Altiplano crust, Bolivia. *Geology, 22*(11), 1003–1006. https://doi.org/10.1130/0091-
1088 7613(1994)022<1003:CATOTS>2.3.CO;2

1089 Zehnder, A. T., & Allmendinger, R. W. (2000). Velocity field for the trishear model. *Journal of*
1090 *Structural Geology, 22*, 1009–1014.